CHEMICAL REVIEWS

pubs.acs.org/CR

Review

Printability and Shape Fidelity of Bioinks in 3D Bioprinting

Andrea Schwab, Riccardo Levato, Matteo D'Este, Susanna Piluso, David Eglin, and Jos Malda*

Cite This: *Chem. Rev.* 2020, 120, 11028–11055

Read Online

ACCESS | Metrics & More | Article Recommendations

ABSTRACT: Three-dimensional bioprinting uses additive manufacturing techniques for the automated fabrication of hierarchically organized living constructs. The building blocks are often hydrogel-based bioinks, which need to be printed into structures with high shape fidelity to the intended computer-aided design. For optimal cell performance, relatively soft and printable inks are preferred, although these undergo significant deformation during the printing process, which may impair shape fidelity. While the concept of good or poor printability seems rather intuitive, its quantitative definition lacks consensus and depends on multiple rheological and chemical parameters of the ink. This review discusses qualitative and quantitative methodologies to evaluate printability of bioinks for extrusion- and lithography-based bioprinting. The physicochemical parameters influencing shape fidelity are discussed, together with their importance in establishing new models, predictive tools and printing methods that are deemed instrumental for the design of next-generation bioinks, and for reproducible comparison of their structural performance.

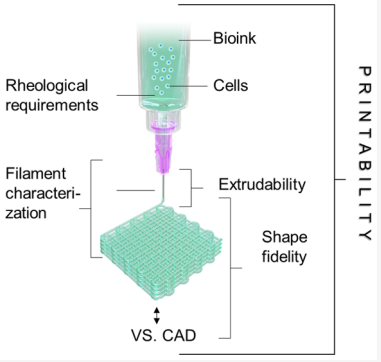

CONTENTS

1. INTRODUCTION

Additive manufacturing (AM), applied to the fields of tissue engineering and regenerative medicine, is a powerful technology for the generation of tissue and organ-like structures. Such structures can be used for transplantation or as predictive, diagnostic, and explorative in vitro models.[1−4]

Biofabrication, including three-dimensional (3D) bioprinting, uses an array of AM derived technologies to create cell-containing objects[5−8] with high resolution and hierarchical organization. Biofabrication has been defined as "the automated generation of biologically functional products with structural organization from living cells, bioactive molecules, biomaterials, cell aggregates, such as microtissues, or hybrid cell-material constructs, through bioprinting or bioassembly and subsequent tissue maturation processes".[9] Interestingly, there has been an exponential growth of published work

Special Issue: 3D Printing for Biomaterials

Received: January 31, 2020
Published: August 28, 2020

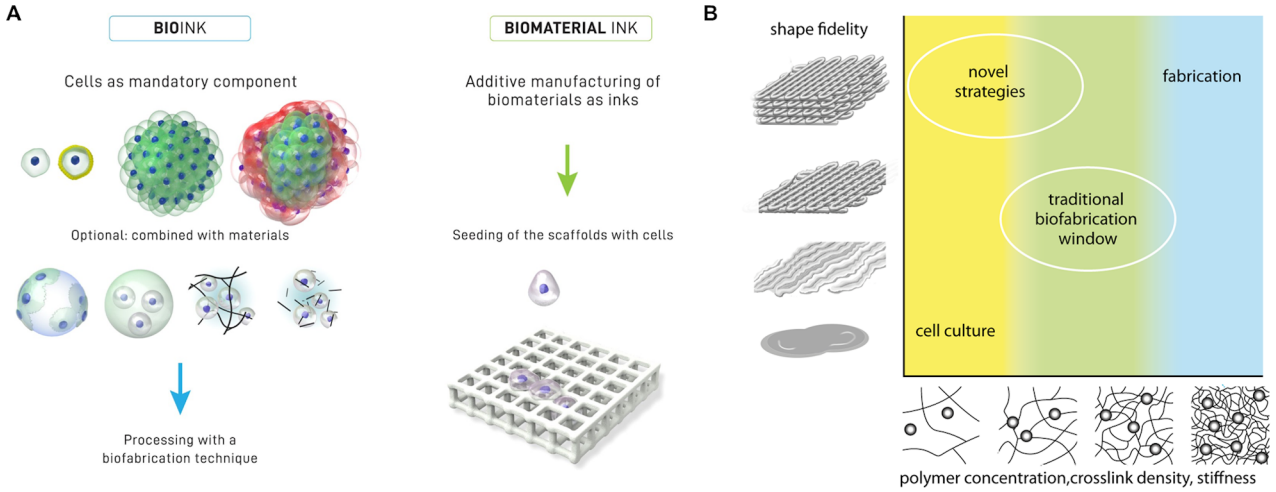

Figure 1. Terminology of cell-free and cell-containing hydrogel inks for bioprinting and the biofabrication window. (A) Distinction between bioinks (cell laden) and biomaterial inks (cell free). In bioinks (left side), single cells, coated cells, and cell aggregates are intrinsic components of the formulation in combination with microcarriers, embedded in microgels, in precursors or physical hydrogels. In biomaterial inks (right side), cells are introduced within the 3D printed biomaterial scaffold, reducing the biological constraints on the inks. (A) Reproduced with permission from ref 20. Copyright 2018 IOP publishing under CC BY 3.0 (https://creativecommons.org/licenses/by/3.0/). (B) Schematic representation of the biofabrication window, illustrating the relation between shape fidelity and polymer concentration, cross-linking density, and stiffness. While stiff materials generally result in high shape fidelity, indicators of biological performance, such as cell proliferation, migration, and differentiation, are commonly reduced in such highly cross-linked hydrogels. The traditional biofabrication window is the result of a compromise between these opposing requirements. Novel approaches have been recently developed that expand the biofabrication window, enabling high shape fidelity even when printing low stiffness materials, enhancing biological competency. (B) Reproduced with permission from ref 21. Copyright 2013 John Wiley and Sons.

related to biofabrication in the last 10 years, with particular focus on extrusion- or light-based bioprinting to generate relatively large, centimeter-scale objects,[4,10−13] with resolutions down to the 10 μm scale.[14,15] Such ability to resolve microscale features while still allowing rapid fabrication times, which can be measured through a "resolution/time of manufacturing (RTM)" ratio, is considered beneficial for a broad range of tissue engineering applications.[5] With these techniques, patient-specific constructs or implants that match the geometrically complex and irregular shapes of the native tissue can be readily produced from computer designs or medical images. In addition, structures with convoluted and customizable internal pore networks can be created, which can, for example, be tuned in pore size and interconnectivity to facilitate nutrient diffusion to sustain the embedded cells.

Extrusion-based 3D-bioprinting approaches encompass the deposition of filaments (in literature sometimes also referred to as strands[16,17] or struts[18]) of a printable cell-containing formulation, which is loaded into a cartridge. Driven by compressed air or a mechanical screw, the formulation or "ink" is then pushed through a nozzle or needle, after which it is deposited onto a building platform in a layer-by-layer fashion.[9,19]

Inks for biofabrication can be distinguished into bioinks and biomaterial inks (Figure 1A).[20] Bioinks contain living cells and are mainly based on aqueous and hydrogel precursor formulations in which the cells are dispersed. To provide a suitable niche for cells to thrive, such hydrogels are typically characterized by low elastic modulus and biochemical composition compatible with cell-driven remodeling. On the other hand, biomaterial inks do not contain living cells, dictating less stringent physicochemical demands and thus allowing for a much wider window of processing parameters, e.g., higher temperatures and pressures and the presence of organic solvents.

One of the enduring challenges associated with bioprinting is the development of bioink formulations that fulfill the physicochemical requirements for their application in AM, as well as the biological requirements associated with the processing of the embedded cells. To highlight this central issue in the field, the "biofabrication window" concept was introduced in 2013 (Figure 1B) by Malda et al., illustrating the dependency of shape fidelity and thus resolution to the polymer concentration and cross-linking density in extrusion bioprinting.[21]

On the basis of studies investigating geometrically organized constructs, it is generally accepted that proper control over the resolution of the resulting printed structures are key for achieving (biologically) functional tissues.[5,22] Therefore, it is of crucial importance that the printed objects closely match the original computer-designed object. However, to make bioinks amenable to bioprinting, the environmental stimuli and forces applied during printing and their impact on the viability and biological performance of the embedded cells must be well understood. This creates an additional layer of complexity in comparison to the use of conventional material-only printing techniques.

Therefore, this review first introduces extrusion-based bioprinting, highlighting its specific bioink requirements. Then, it summarizes and discusses the currently applied methods for the assessment of printability, including the analysis of extrudability, shape fidelity, and filament characterization, to aid the reader in the selection of methods to evaluate the structural performance of novel bioinks. This is followed by an overview of approaches to counteract the specific forces and physical events that may potentially have detrimental effects on shape fidelity in extrusion-based

https://dx.doi.org/10.1021/acs.chemrev.0c00084
Chem. Rev. 2020, 120, 11028−11055

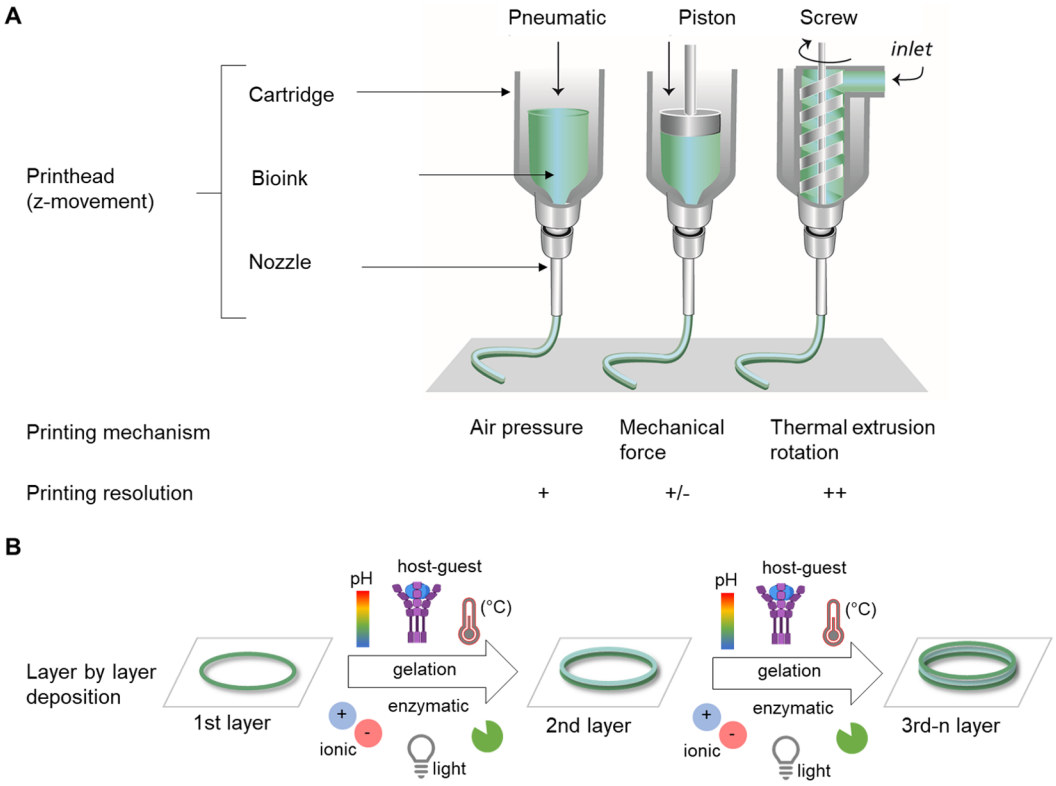

Figure 2. Extrusion-based bioprinting. (A) Schematic illustration of extrusion printing technique: pneumatic, piston, and extrusion driven printing. Adapted with permission from ref 21. Copyright 2013 John Wiley and Sons. (B) Bottom up approach with layer-by-layer deposition of a bioink to produce 3D scaffolds, including gelation (e.g., light, ionic, pH, temperature, host−guest interaction, enzymatic) between deposition of single layers.

printing. Further, lithography-based bioprinting techniques are introduced, together with the implications of the concepts of printability and shape fidelity in such nozzle-free approaches. Overall, the importance of introducing novel, quantitative tests, as well as the development of predictive models based on rheological and chemical parameters of the inks is also discussed as a new toolkit in the design of the next generation of bioinks.

2. EXTRUSION-BASED BIOPRINTING: MANUFACTURING TECHNOLOGY AND MATERIALS

2.1. Extrusion-Based Bioprinting

Extrusion-based bioprinting represents one of the most commonly used techniques to fabricate relatively large tissue constructs with high densities of cells.[23−26] The working principle of extrusion bioprinting is similar to that of polymer-based fused deposition modeling (FDM) rapid prototyping processes.[5] In FDM, the feed material is extruded through a nozzle and the molten polymer is then shaped to its desired geometry in a layer-by-layer fashion. Extrusion bioprinting plots filaments of a hydrogel-based bioink and the imposed shape is fixed upon cross-linking of the hydrogel precursor, for example, via pH or temperature changes, ionic cross-linking, photochemical reactions, enzymatic cross-linking, and guest−host interactions (Figure 2B). Despite their great potential and versatility, extrusion-based techniques use filaments as building blocks, which complicates the creation of more complex, convoluted architectures, especially when aiming to print overhangs and out-of-plane features, the latter referring to filaments not aligned along a single plane when printing following Cartesian coordinates, as previously described.[27] For a more detailed description of the extrusion-based bioprinting process, we refer the reader to other excellent reviews in the field.[24,28]

Extrusion-based systems can be piston-, pneumatic-, or screw-driven (Figure 2A). The screw-driven system is particularly suitable for the extrusion of highly viscous materials, e.g., with viscosities up to 10^4 Pa·s,[29] and mainly used for the printing of thermoplastic polymers, e.g., for poly(ε-caprolactone) (PCL). The cell-containing hydrogel can either be cast within the printed thermoplastic structure or be co-printed in a multitechnology fabrication process[30−32] to yield structures with increased mechanical stability.[33−37] For printing materials with lower viscosities (<10^7 mPa·s)[38] compared to screw-driven extrusion, piston- or pneumatic-based extrusion systems are typically used. Many commercial bioprinter set ups are based on pneumatic dispensing, which is highly versatile, but tend to provide lower control over the deposition of inhomogeneous inks, such as certain particulate composites and slurries.[39]

To allow for the controlled deposition of a variety of inks, such set ups are more often modular and equipped with multiple printheads, cooling and heating systems, and light sources to control gelation. However, rapid switching between multiple cartridges is a necessity to effectively combine different inks within a single construct, as well as to establish interfaces and gradients of different materials and cell types.[31,40]

Although tool heads with accuracies in the $x-y-z$ planes ranging from 5 to 100 μm are readily available, the actual printing resolution of deposited structures is mainly dictated by the ink and the nozzle diameter. In case of bioinks, the

https://dx.doi.org/10.1021/acs.chemrev.0c00084
Chem. Rev. 2020, 120, 11028−11055

resolution is typically limited and in the range of hundred micrometers to millimeters, as shear stresses at the dispenser tip, which inversely correlate with the nozzle diameter, should be minimized to prevent damage to the embedded cells.[41−46] In contrast, resolutions obtained with biomaterial inks are much higher as these are not limited by such constraints, and can be extruded through thinner microneedles with higher pressures.

2.2. Materials and Cross-Linking Strategies for Extrusion-Based Bioprinting

Hydrogel precursors with the ability to be extruded through a small-sized nozzle and subsequently forming shape-stable gels are suitable for extrusion-based printing. Natural hydrogels, such as alginate,[42,47−50] agarose,[51−53] collagen,[54−56] gelatin,[49,57−60] fibrin,[31] decellularized extracellular matrix (dECM),[61−63] hyaluronic acid (HA),[64−67] or silk[68−70] have been extensively used as bioink components due to their structural similarities to the native ECM. Further, hydrogels based on collagen,[71,72] gelatin,[73,74] or fibrin[75,76] possess inherent signaling molecules that favor cell adhesion. However, their mechanical properties are generally weak. In contrast, synthetic materials, such as polyethylene glycol (PEG)[77] and poloxamers,[78] are often used due to their tunable mechanical properties and lower batch-to-batch variability.[79,80] These materials lack bioactive molecules to promote cell adhesion and migration, as well as enzyme-mediated degradation and remodeling. This limitation can be overcome by functionalization of the materials, for instance, with bioactive peptides.[81−86] Both natural and synthetic materials have been modified with functional groups to enable cross-linking and to stabilize the extruded ink. For example, gelatin and HA have been modified with methacrylate groups or other functional groups, such us tyramine, norbornene, thiols, vinyl sulfone, or aldehyde.[79,80] More in-depth discussions on the wide array of bioinks available and on the design requirements for biomaterial inks and bioinks are out of the scope for the current review, thus we refer the reader to other excellent contributions to the literature.[23,28,79,87−93]

To prevent excessive shear stresses that can affect the survival of cells during the printing process,[42−46,94] hydrogel-based inks with shear-thinning properties are often used, as for these materials the viscosity is reduced during extrusion. Alternatively, solutions containing hydrogel precursors are used, as these possess viscosities lower than the final hydrogel after gelation. Pregels give rise to molecular networks based on physical cross-linking due to the presence of ionic or hydrogen bonds or due to hydrophobic interactions between the polymer chains. For example, alginate-based formulations have been used as bioinks with ionic cross-linking through direct extrusion into a calcium solution. A low amount of divalent ions can also be used to modulate the initial viscoelastic properties of alginate-based bioinks.[95] Physical cross-linking based on hydrogen bonding or hydrophobic interactions is often temperature dependent, therefore temperature changes will affect the rheological behavior of the ink.[96] This is the case for inks based on methylcellulose,[42,97] gelatin,[50,98] alginate,[99,100] and Pluronic.[101,102] The use of jammed gels, which are densely packed microgels, is also an alternative approach to overcome the exposure of the cells to excessive shear stresses during printing, as these form a colloidal-like suspension.[93,103,104]

Once the material exits the nozzle, it should retain the imparted shape without deforming or flowing. To improve homogeneous and stable filament extrusion, precross-linking strategies can be employed to adjust the rheological properties of the ink.[105] This can be achieved in different ways, e.g., through enzyme-mediated cross-linking, guest−host interactions or through physical mechanisms.[57] The precross-linking step is followed by a second cross-linking after printing. Both cross-linking steps can be based on different chemistries and mechanisms. For instance, shear-thinning hydrogel obtained through supramolecular self-assembly mediated by guest−host interactions between adamantane and β-cyclodextrin were stabilized with a secondary cross-linking based on Michael addition.[106,107] For the stabilization of extruded filaments, one of the most commonly used mechanisms is photoinduced cross-linking. In this case, photoinitiators are added to the bioink formulation. These molecules, upon exposure to light, produce reactive species that trigger the polymerization process.[57,108−112] Most photo-cross-linkable systems rely on ultraviolet A (UV-A) and visible light irradiation at wavelengths that do not directly cause significant DNA damage.[113,114] These approaches make use of commonly used photoinitiators and photosensitizers (e.g., Irgacure 2959,[115,116] lithium phenyl-2,4,6-trimethylbenzoylphosphinate,[116,117] Eosin Y,[118] ruthenium/sodium persulfate,[119] and rose Bengal[120]). Photo-cross-linking in extrusion printing can be applied after deposition of each layer or after completion of the entire print, the latter requiring better shape retention of the ink. However, in both cases, the complete prevention of filament collapse still remains a challenge.[119,121]

Alternative cross-linking methods for a broad variety of natural and synthetic hydrogels, involve the use of enzymes such as sortase, transglutaminase, tyrosinase, lysil oxidase, phosphatase, or peroxidase.[122,123] Horseradish peroxidase (HRP) is widely used and requires the presence of hydrogen peroxide (H_2O_2) for the oxidative coupling of phenol derivatives.[124] The HRP and H_2O_2 concentrations dictate the viscoelastic properties of the formed polymeric network and rheological properties of the obtained ink.[105,125] For a more detailed overview on the cross-linking mechanisms, we also refer the reader to other notable reviews.[57,79,109−111,126]

3. RHEOLOGICAL FACTORS AFFECTING PRINTABILITY AND SHAPE FIDELITY

Rheological properties are the physicochemical parameters with the largest influence on hydrogels printability. Rheology describes the deformation and flow of materials under the influence of applied forces.[127] In 3D extrusion-based processes, a bioink initially present in a bulk resting state, undergoes a transition to a high shear condition while passing through the nozzle, takes a new shape, and finally reaches a new resting state. The key rheological properties describing these transitions are viscosity, viscoelastic shear moduli, elastic recovery, and shear stress.[78]

Viscosity is the resistance of a fluid to flow under the application of stress and has a great influence on both the print fidelity and efficiency of cell encapsulation. Generally, higher viscosities result in higher printing fidelity. However, high viscosity also leads to increased shear stress, which can affect the cells suspended in the bioink. The main factors determining the viscosity of polymers in solution are molecular weight and concentration.[127] Viscosity is defined as the ratio of the shear stress to the shear rate. Fluids showing a linear

https://dx.doi.org/10.1021/acs.chemrev.0c00084
Chem. Rev. 2020, 120, 11028−11055

relationship between shear stress and shear rate are termed *Newtonian*. Fluids exhibiting deviations from linearity, with either decreasing or increasing ratios are defined *non-Newtonian*. *Non-Newtonian* fluids can be classified into time-independent (e.g., shear-thinning and shear thickening) and time-dependent fluids (e.g., thixotropic or rheopectic).[127,128]

3.1. Shear-Thinning

Shear-thinning is the most common type of time-independent *non-Newtonian* fluid behavior, where increasing shear rates result in a decrease of viscosity. This property is typically exhibited by materials often used in extrusion printing, such as polymer melts, polymer solutions above a critical concentration, partially cross-linked hydrogels, and colloidal suspensions.[129]

In extrusion printing, shear-thinning is related to the ease of extrusion in combination with initial shape preservation of a bioink, with a decrease of viscosity during the extrusion phase, where the shear forces dramatically increase.[130] After extrusion, the shear rate drops with a corresponding rise in viscosity, thereby contributing to preserve the printed shape. The higher the zero-shear viscosity, the slower the flow and deformation of the material will be preventing the printed structure to collapse during the time for the secondary cross-linking to occur. For example, high zero-shear viscosity contributes to the shape preservation in printing calcium phosphate cements.[131−133]

The molecular mechanisms behind shear-thinning and the physicochemical interactions giving shape retention are different for distinct classes of bioinks. Polymers commonly employed for FDM, such as PCL and polylactic acid (PLA), give melts which are intrinsically shear-thinning due to shear-induced disentanglement of the long polymeric chains.[129] High molecular weight polymers are entangled and randomly oriented at rest. Upon shearing, the polymer chains disentangle and align causing a decrease of internal resistance and thereby of viscosity. For these bioinks, shape retention is triggered by the abrupt transition from a melt to a solid state.

For bioinks based on colloidal dispersions, pastes and solid suspensions, shear-thinning arises from the shear-induced disruption of the interactions between the solid particles. The relatively high viscoelasticity at rest, determined by the re-establishment of interactions between the suspended particles, ensures shape stability. Notable examples belonging to this category include polymer solutions containing dispersions of nanosilicates, often used as biomaterial inks or bioinks,[134−137] and calcium phosphate cements.[138,139] For these bioinks, the setting reaction further contributes to the shape fixation after printing.

Finally, pregel solutions or partially cross-linked hydrogels are shear-thinning due to polymer disentanglement and macromolecular orientation along the shear flow. This mechanism is similar to that of polymer melts, with the important difference determined by the presence of the solvent.[129] Although elastic recovery and yield stress are often observed, for this category of bioinks, the long-term shape stability is typically given by a secondary cross-linking after printing.[140]

Another class of time-independent fluids are shear-thickening or dilatant materials. They are characterized by an increase in viscosity with increasing shear rate, a property generally not relevant for printing applications. *Non-Newtonian* materials can exhibit a time- rather than shear-dependent viscosity. For thixotropic materials, the viscosity decreases with time at constant shear rate, returning to its original value after a period of rest. The opposite behavior is termed rheopectic and is characterized by an increase of viscosity as a function of time and shear rate.[127] In general, time-dependency of the viscosity profile may render extrusion printing more complex and thus is not usually sought during ink design, as printing parameters, such as extrusion pressure, would need to be continuously adjusted to preserve a constant flow of the material.

3.2. Viscoelasticity and Yield Stress

Bioinks for extrusion printing display both flow and shape-retention properties. While passing through a nozzle, inks should flow with minimal internal resistance, especially in the presence of cells. After the material has been dispensed the properties should be opposite, with immediate flow discontinuation, buildup of internal forces opposing to deformation, and elastic shape retention. The property of displaying viscous flow and elastic shape retention is known as viscoelasticity. This behavior can be described using two parameters: the storage (or elastic) modulus G' and the loss (or viscous) modulus G''. The storage modulus G' is a measure of the amount of energy elastically stored during deformation and therefore is associated with elastic shape retention. The loss modulus G'' measures the amount of energy dissipated by the material and therefore is linked to the viscous flow. Viscoelastic properties can be determined via oscillatory rheology, in contrast to viscosity which is measured under rotation. G' and G'' are typically measured as a function of the frequency and amplitude of the oscillation.[129] The G''/G' ratio is designated as damping factor, loss tangent or tan(δ).

Besides storage modulus, shape retention can also be described in terms of the yield point. The yield point (or yield stress) is the stress that has to be exceeded for deformation to occur (Figure 3B). Both elastic modulus and yield point are correlated to the number of cross-links or entanglements within the bioink. These interactions provide

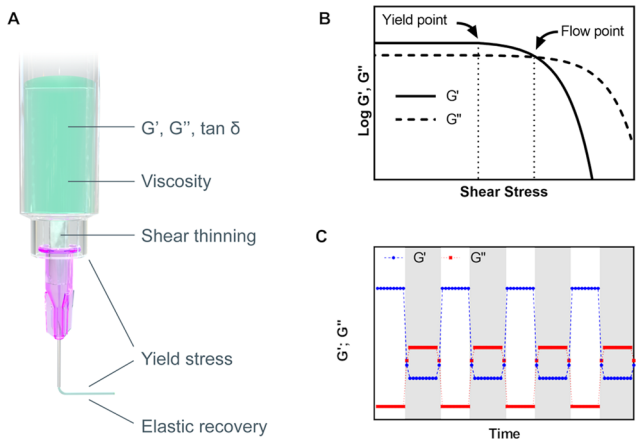

Figure 3. Rheological properties affecting printability and shape fidelity. (A) Interplay of rheological properties in extrusion-based printing. (B) Amplitude sweep of a viscoelastic substance represented as a function of the shear stress, illustrating the yield point as the limit of the linear viscoelastic range, and the flow point, e.g., the stress at which the viscous modulus G'' is above the elastic modulus G' and therefore flow can occur. (C) Elastic recovery test, where G' (blue) and G'' (red) are measured under low deformation (white time interval) and high deformation (gray time interval). The curve represents the idealized behavior of a bioink for good printability and shape retention.

https://dx.doi.org/10.1021/acs.chemrev.0c00084
Chem. Rev. 2020, 120, 11028−11055

internal resistance against change in shape, such that for small perturbations the material behaves like an elastic solid recovering the original shape, whereas above a certain threshold the material is deformed permanently, e.g., it yields (yield point) or flow occurs (flow point). The yield point can also be assessed based on the viscous properties in rotational rheology, however, in this case, the measurement is subject to instrumental bias, and therefore the determination in oscillatory rheology is recommended.[129]

Increased yield stress of an ink generally improves filament formation and stiffness of the final construct, but it can also hinder cell encapsulation. Gellan gum, hyaluronan, or carrageenan are typical examples of additives that increase the yield stress of a given ink.[141,142] For instance, the addition of gellan gum to gelatin methacryloyl, in the presence of cations in solution, induces the formation of a shear-reversible ionically cross-linked network, which, at rest, results in an increase of viscosity of the ink. Such reversible network is broken by shear forces during dispensing and it reforms after the shear forces are removed.[141] A deposited material with sufficient yield stress or elastic properties will not flow unless the acting forces overcome this yield threshold value; these forces include gravity, determined by the filament own weight and by the weight of all layers above it, capillary forces, and surface tension.[78]

Another fundamental aspect is the transition kinetics from fluid-like flow to elastic shape retention. This property can be quantified by measuring the recovery of the shear moduli[104,143,144] or the viscosity[144] over time upon removal of stresses above the yield. In Figure 3C, a typical example of material recovery is illustrated, where the bioink undergoes an oscillatory test with small deformation, followed by a large and destructive deformation (gray time interval). In this example, the bioink displays a profile supporting good printability: for small deformations, there is a clear elastic prevalence $G' \gg G''$, whereas with the destructive deformation representing extrusion, the prevalence is viscous $G'' > G'$; additionally, the transition between the regimens should be ideally instantaneous over several cycles.

While rheological properties and in particular shear-thinning behavior and rapid, reversible sol−gel transition are key factors in defining printability and shape fidelity in extrusion printing, the rheological requirements for lithography-based bioprinting are widely different. In stereolithography (SLA) and dynamic light processing (DLP), the ideal biomaterial should display low viscosity, as a new volume of the materials needs to effortlessly flow under the building platform after each layer is cross-linked, ideally even in the absence of a mixing mechanism, as further discussed in section 5 of this review.

3.3. Embedding of Cells Affects the Rheological Properties of the Bioink

While the viability and proliferation of cells embedded within a bioink is an important aspect, the impact that cells have on the physicochemical properties of the ink has been often overlooked. Cells within a bioink occupy a specific volume, depending on their size and density. The volume taken up by cells is precluded to the hydrogel, potentially impacting on the cross-linking efficiency and viscoelastic properties.[60] In fact, cells can interfere with the cross-linking, acting as a physical hindrance between different regions of the ink or limiting contact between reacting groups. This was observed when loading cells in a HA-based bioink. At a cell density up to 25 × 10^6/mL, the gelation time was comparable to the cell-free ink; however, a cell density of 100 × 10^6 cells/mL resulted in an increased gelation time (from 20 min to 1 h), whereas cell densities of 250 and 500 × 10^6 cells/mL fully prevented gelation from occurring.[145] Further, the presence of cells (2.5 × 10^6 cells/mL) resulted in a decreased viscosity (4-fold) of gelatin methacryloyl bioink compared to cell-free ink.[146]

Another phenomenon to consider is that upon adding cells the bioink effectively turns into a composite material. Thus, high densities of cells suspensions behave as colloidal systems displaying shear-thinning and ultimately printability, even in the absence of rheological enhancers or additional biomaterials.[4,147,148] Cells have characteristic mechanical properties; for example, chondrocytes were reported to have a (pseudo) Young modulus of 0.6 kPa[149] as measured via a combined experimental and theoretical approach consisting in micropipette aspiration, finite elements models, and 3D confocal microscopy to determine the deformation in situ. The cell influence on the viscoelastic properties of the bioink is further complicated by the fact that cells may be surrounded by pericellular matrix, modifying their mechanical properties,[150] hydrodynamic radius, and boundary conditions at the fluid interface.

As such, the effects of cells laden in the ink do not result in straightforward alterations of the rheological properties. For example, in a collagen-based bioink, high cell density (up to 100 × 10^6 cells/mL) increased the viscoelasticity of the precursor hydrogel while decreasing the storage modulus after gel formation. Additionally, high cell densities slowed down the kinetics of the gel formation.[54] The influence of cell encapsulation on the rheological properties was also investigated for bioinks consisting of mixtures of a thermoresponsive HA with the methacrylated derivative of either HA or chondroitin sulfate.[16] The rheological properties before and after thermal gelation and, following UV-mediated cross-linking, were markedly different for the two compositions. Below thermal gelation, cell addition resulted in lower G' and G'' for the chondroitin sulfate derivative, while both moduli increased for the HA derivative; after thermal gelation and UV cross-linking, the moduli were almost unvaried for the chondroitin sulfate derivative and markedly higher for the methacrylated HA. Similar reaction conditions were used for both inks, suggesting that the volume occupied by cells is not the only factor affecting the resulting rheological properties.

When different cross-linking mechanisms are involved, striking differences on the impact of cell encapsulation can be observed. Encapsulation of up to 9 × 10^6 cells/mL had little or no impact on the viscosity of pentanoate-functionalized HA as a bioink.[151] On the contrary, the presence of cells had a dramatic impact on the rheological properties of a HA-tyramine based bioink, turning it from a shear-thinning soft gel when cell free ($G' > G''$) to a runny unprintable liquid ($G'' > G'$) when the cell density reached 5 × 10^6 cells/mL.[125] In this case, cells were likely responsible for hydrogen peroxide inactivation, depriving the enzymatic reaction of this reagent, thus resulting in less cross-linking.

In fact, cells may even actively participate to and interfere with the chemical processes driving the cross-linking reactions. For example, cells might capture free-radicals generated from photoinitiators or internalize small molecules making them not available for chemical cross-linking.[125] Interestingly, for the enzymatic gelation of HA-tyramine, it was observed that the cell-induced decrease in viscoelastic properties diminishes at

https://dx.doi.org/10.1021/acs.chemrev.0c00084
Chem. Rev. 2020, 120, 11028−11055

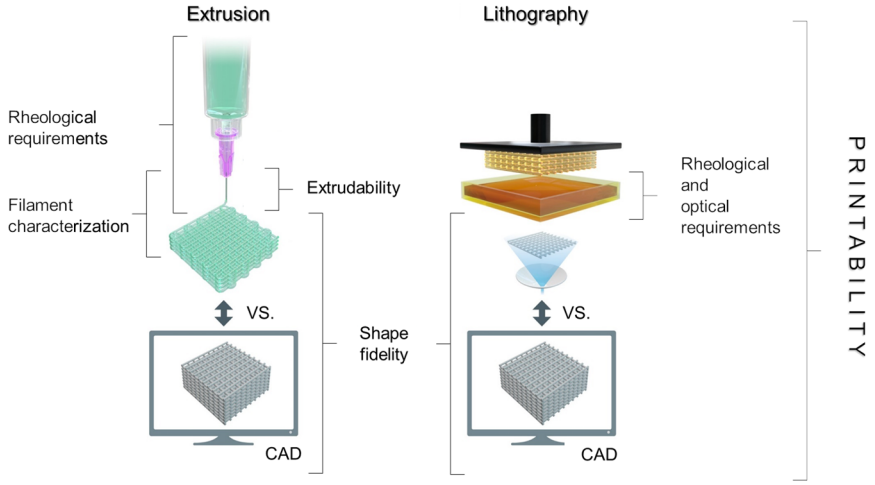

Figure 4. Key aspects to assess printability in the context of extrusion- and lithography-based bioprinting technologies. While the principles (e.g., extrudability, filament characterization, rheological requirements) to assess the printability of a given bioink for extrusion-based bioprinting are different from those needed for lithographic bioprinting, the definition and methods to assess shape fidelity remain comparable across these different bioprinting platforms.

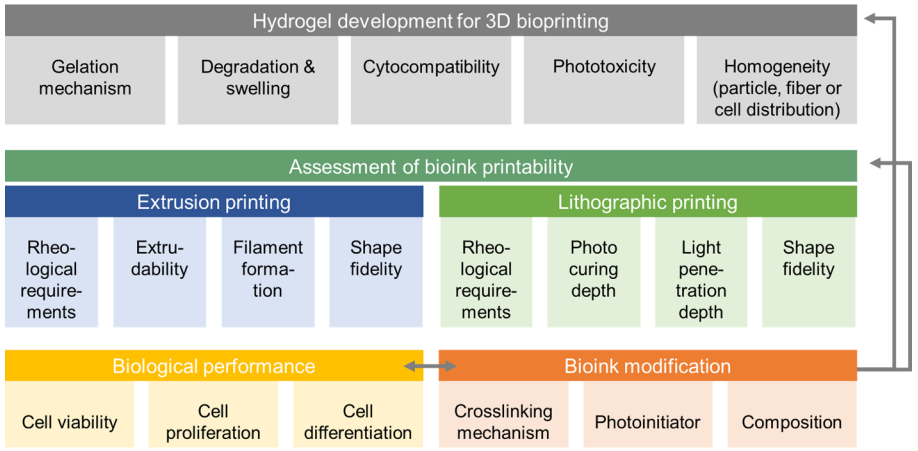

Figure 5. Schematic summarizing key aspects during bioink development and modification, including printability assessment. During hydrogel development for 3D bioprinting, a cell friendly gelation mechanism and biomaterial cytocompatibility need to be assessed. When cells, particles, or fibers are embedded in the biomaterial, a homogeneous distribution before and after gelation is desirable to minimize sedimentation. Degradation and swelling behavior may have an influence on geometrical accuracy. The second step covers the assessment of printability which differs between printing technologies. The concept of printability assessment for extrusion printing includes rheological characterization, extrudability, and filament formation as well as shape fidelity. In lithographic printing, rheological requirements, shape fidelity is accompanied by optimization of photocuring depth and light penetration depth. After optimizing printing parameters to meet the printability requirements, the biological performance, including evaluating cell viability, cell proliferation, and cell differentiation, is required. When the bioink is modified by means of composition, cross-linking mechanism, or photoinitiator, the whole workflow should be repeated to ensure a cell friendly environment and optimized conditions to achieve good printability.

lower temperature, and the extent of this effect appears to vary with the embedded cell type.[152] This suggests that uptake and neutralization of reactive species might depend on the metabolic activity of the cells. A further aspect is that certain cross-linking chemistries, such as phenol−phenol coupling, thiol−ene or aldehyde-based systems, such as hydrazine-forming inks,[153,154] involve functional groups which are naturally present on amino acids and thereby on the cell surface.[155−159] Besides considering the impact this can have on cell viability and metabolism at high cell density, it may even occur that cells could provide molecular material to bridge the bioink molecules.

The above evidence underlines how the impact of cells on bioink properties is manifold. Important phenomena to be considered include volume exclusion, alteration of viscoelastic properties due to the cells in suspension, and potential interference of cells with chemical processes. The extent of these effects depends also on the metabolic state of the embedded cells, their subtype, encapsulation density, and occupied volume, with potential difference when single cells, spheroids, or complex aggregates are processed. Given that biofabrication is a field still in its infancy, future studies can be envisioned to unravel the impact on shape fidelity and printability of cells as printable materials, both from a physical and biological point of view.

4. ASSESSMENT OF PRINTABILITY AND SHAPE FIDELITY

Assessment of printability and shape fidelity is a crucial step in the development a bioink. Although "printability" is a widely

https://dx.doi.org/10.1021/acs.chemrev.0c00084
Chem. Rev. 2020, 120, 11028−11055

Table 1. Parameters and Approaches Introduced To Evaluate Printability in Extrusion Printing. Data Focus on Materials Properties Pre-Printing as Well as on the Printing and Optimization of Filament Formation and Shape Fidelity of Single (1−2) Layers[a]

methodology	parameter	significance	remarks	ref
rheology	flow behavior	shear-thinning behavior indicated by decrease in viscosity at increasing shear rate	• characterization of the bioink during development and optimization for printing • absolute magnitude independent of the printer type • provides an input parameter for in silico models	17, 48, 65, 105, 144, 151, 168, 203, 204
	yield stress	can counter deformation from gravity or surface tension, potential predictor of how well an ink holds its shape after extrusion	• absolute magnitude independent of the printer type • provides an input parameter for in silico models	78, 141, 144, 151, 205
	elastic recovery	time dependent response of the material after shear induced deformation	• absolute magnitude independent of the printer type • predicts filament recovery upon extrusion out of the nozzle	48, 104, 143, 144, 151, 168, 203, 206
	shear stress	affects both cell behavior and printing resolution	• absolute magnitude independent of the printer type • provides an input parameter for in silico models	43, 45, 60, 207
	damping factor = tan (δ) = loss tangent	identifies a suitable balance between flow and shape retention	• dimensionless parameter based on rheological data • independent of printer • comparable across laboratories	105, 125, 162, 163
filament formation	filament formation	drop vs continuous flow formation upon extrusion	• posthoc feedback to optimize printer settings • requires pregel with yield point	42, 46, 144, 169, 170
	filament uniformity	fidelity of filament geometry (diameter, height, aspect ratio) as a predictor of shape fidelity	• strategy to optimize printing settings • neglects layer stacking • requires pregel with yield point	46, 58, 62, 105, 134, 140, 163, 171, 178, 180, 182, 183, 187, 208
	filament collapse	stability of a single filament to bridge a distance without sagging	• prefabrication screening • estimates potential artifacts and pore closure in the z-direction	42, 78, 172, 174
	filament collapse + gravity	stability of multiple filaments to bridge a distance	• limited to pregels with yield point • filament circularity and layer stacking is neglected • limited to single layer constructs • distance to bridge is related to printing geometry	175
	filament fusion	defines the pore closure of two filaments	• time dependent ink flow in delayed of postextrusion cross-linking • filament spacing is dependent on substrate surface	78,176
extrudability	extrusion force	defines force needed to extrude an ink out of a nozzle	• extrusion force measurement to define pressure to achieve homogeneous flow • investigation of ink homogeneity during extrusion	60, 140, 168, 179, 208

https://dx.doi.org/10.1021/acs.chemrev.0c00084
Chem. Rev. 2020, 120, 11028−11055

Table 1. continued

methodology	parameter	significance	remarks	ref
in silico models	power-law model	numerical model considering rheological data (viscosity shear rate) and printing parameters (needle length and radius, extrusion pressure and velocity) to predict shear-thinning coefficients	• restricted to static and linear fluid flow • restricted to incompressible materials • empirical model	144
	Herschel−Bulkley equation	numerical model considering rheological data (shear stress, shear rate) to predict flow behavior, flow rate and yield stress	• applicable for non-Newtonian fluids • considering nonlinear shear stress and shear strain behavior • includes wall slipping (reduced viscosity near needle wall) • empirical model	100, 166
shape fidelity	filament circularity	describes filament spreading on a surface	• directly related to geometry of macroscopic shape • applicable to single and multilayered constructs to identify how well layers are stacking	46, 105, 140
	pore geometry	degree of reproducing ideal geometrical shapes	• applicable for horizontal and transversal pores in multi layered constructs • pore geometry is related to filament spreading and fusion at intersection • limited to open pore structure	46, 55, 163, 180, 188, 206
	visual grid	direct comparison of printed structure to computer generated lattice	• limited to simple constructs with macroscopic porosity	46, 105, 178, 183, 209
combined methodologies (image analysis, rheology)	biofabrication window	multiple parameter analysis to visualize parameter interplay	• phase diagram based only on selected parameters • readability limited to 3D graph illustrating maximum of three parameters • for multiple parameters visualization e.g., radar plots are possible	21, 38, 46, 126, 141, 144, 210, 211
dimensionless indices and scores	integrity index/ printing fidelity	relative evaluation of layer stacking	• related to merging filaments and filament collapse (values <1) • percentage of height relative to theoretical height	55, 105, 162, 163
	shape fidelity score	qualitative evaluation of printed grid and scoring based on edge shape and retaining of structure	• indices and scores solely focus on quality of printed filaments • should be combined with scores addressing further analytics related to printability	62,151
	printability index	relative evaluation of pore geometry	• related to filament merging and collapse (P_r < 1) • index focuses on transversal pore geometry	42, 46, 170, 187−189

[a]Parameters are summarized based on the methodology (rheology, image analysis, dimensionless indices and scores, numerical models).

used term in biofabrication-related literature, there is currently no clear consensus on when a material or formulation is considered "printable". Gillispie et al. defined printability as "the ability of a material, when subjected to a certain set of printing conditions, to be printed in a way which results in printing outcomes which are desirable for a given application".[160] Hence, the evaluation often relies on diverse parameters of the printing process, which hamper comparability between inks used in individual studies. However, in the framework of extrusion bioprinting, printability generally refers

https://dx.doi.org/10.1021/acs.chemrev.0c00084
Chem. Rev. 2020, 120, 11028−11055

to the "suitable" extrudability, filament formation, and shape fidelity (Figure 4 and Figure 5), which are all parameters indicating the degree of dimensional faithfulness of the printed object in comparison to the designed one. In this context, the term shape fidelity can be used to describe the shape retention of single filaments upon extrusion as well as of the printed construct as a whole compared to the original computer design and is sometimes referred to as print accuracy.[160]

For the evaluation of bioinks for extrusion printing, various approaches can be distinguished, particularly based on how they are related to the different stages of the printing process (pre- and postprinting for example). Importantly, it should be emphasized again that any assessments of the cell-free ink may not hold complete relevance for the equivalent cell containing bioink, as cells have an impact on the rheological properties of the mixture.[16]

During the development of a hydrogel as a bioink, a suitable gelation mechanism, homogeneity of the materials in terms of cell (or if any other fiber or particulate additive) distribution, cytocompatibility, and swelling/degradation behavior need to be investigated and optimized (Figure 5). To assess printability, a first step prior to printing may consist in assessing the key rheological properties of the ink (as illustrated in Figure 3A) as predictors of the potential shape fidelity. Moreover, as hydrogel filaments are the basic building blocks in extrusion bioprinting, the formation (section 4.1), their planar orientation (section 4.3) and stacking during the layer-by-layer printing process (section 4.4) can also be evaluated. The quality and mechanical stability of these filaments is a primary indicator of printing accuracy, shape fidelity, and resolution than can be achieved (Table 1). With advanced imaging technologies, real-time monitoring (section 4.5) of the printing process becomes a feasible strategy for the on-the-fly, direct assessment of both the individually printed layers and assembled 3D constructs. Once a hydrogel or bioink is modified, e.g., by changing composition or gelation mechanism, the whole workflow of printability assessment should be repeated. Finally, and specifically for biofabrication, the assessment of the biological performance of the bioink,[94] should not be neglected, especially assessment beyond the simplistic analysis of cell viability, in order to evaluate the impact of the materials and the printing process on superior cell functions, such as proliferation and differentiation and matrix remodelling postprinting. The optimization of such biological properties may even likely require an iterative optimization of the printing process.

4.1. Rheological Evaluation

The rheological characteristics of a bioink are often used as a predictor of its printability and shape fidelity.[78,144,161] In particular, shear-thinning (section 3.1) kinetics of the elastic recovery and yield stress (section 3.2) are the most frequently evaluated parameters. In general, a first test can be performed to evaluate the rheological properties of a bioink subjecting the material to increasing shear stresses to assess whether a material exhibit a yield stress behavior. The next step is the evaluation of the shear-thinning property by measuring the viscosity of the ink as a function of the shear rate. Finally, recovery tests are performed to analyze the ability of the materials to restore their elastic properties when exposed to alternating high and low shear stress.

Another relevant rheological parameter is the damping factor or tan (δ). Corresponding to the ratio between loss and elastic moduli, tan (δ) carries information on the balance between the viscous and elastic deformation properties. The measurement of the damping factor takes a few seconds and is scarcely prone to experimental bias, thus it is a useful quantitative parameter for quickly screening a bioink.[105,125,162,163] Damping factors between 0.4−0.6 and 0.25−0.45 were reported for tyramine-HA[105,125] and a gelatin−alginate composite,[162] respectively, to yield maximal shape fidelity.

Importantly, because the rheological properties are intrinsic to the material, they can be used to compare results between different laboratories, provided that the same testing protocols are applied. This universal character is useful especially for the comparison of different bioinks independently of the printing device to be used. However, to identify optimal ranges, it is necessary to consider geometrical and instrumental factors. For example, the optimal range of rheological properties for a bioink intended for extrusion printing at 37 °C and 1.5 bar with an 800 μm nozzle, will be different from the optimal range of a bioink extruded through a smaller nozzle diameter or higher pressure, as well as from the optimal range for a bioresin intended for DLP printing.

Mathematical models can be applied to predict the optimal printing conditions (e.g., feed rate, nozzle diameter, or temperature), using as input data measures from the viscosity-shear rate profile of a bioink. Shear-thinning can be quantitatively assessed using a rotational rheometer to measure the viscosity under increasing shear rate. On the basis of the viscosity curves obtained, empirical shear-thinning indexes can be derived from the ratio between viscosities measured at different arbitrarily selected shear rates.[164] Several mathematical models for shear-thinning behavior have been proposed. One of the most used models is the Ostwald−de Waele model or the power law (eq 1), which is defined as[137]

$$\eta = k\dot{\gamma}^{n-1} \tag{1}$$

where η is viscosity, k is a constant called consistency index (defined as the viscosity when the shear-rate is 1 s^{-1}), $\dot{\gamma}$ is the shear rate, and n is the shear-thinning index, also referred to as flow index or power-law index.[137] Shear-thinning index $n < 1$ identifies shear-thinning materials, $n > 1$ shear thickening materials, whereas $n = 1$ designates *Newtonian* fluids.

The extrusion velocity during printing can be calculated from the shear stress (using the following eq (eq 2):[144]

$$\tau = \left(\frac{\delta v}{\delta r}\right)^n \tag{2}$$

where n is the shear-thinning parameter derived from the power law, v is the extrusion velocity of the fluid, and r is the radius of the needle. Considering that the shear stress is proportional to the applied pressure and the radius of the nozzle, the velocity of extrusion for a range of materials and conditions can be determined using the following eq (eq 3):[144]

$$v = \frac{n}{n+1}\left(\frac{\Delta p}{2LK}\right)^{1/n}(R^{n+1/n} - r^{n+1/n}) \tag{3}$$

The power law is a relatively simple model that can be used to predict printability.[126,144] For example, this model has been applied as initial screening to determine the printability of bioinks based on alginate, gelatin−alginate blends,[46] and poloxamer 407.[144] Recently, this model has also been used to predict the shear thinning behavior of nanosilicate/PEG-based bioinks.[165]

https://dx.doi.org/10.1021/acs.chemrev.0c00084
Chem. Rev. 2020, 120, 11028−11055

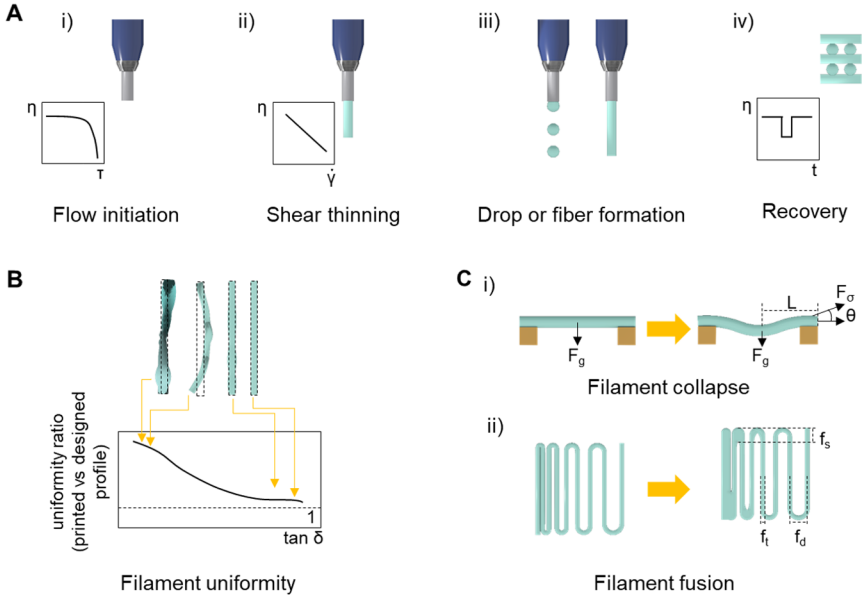

Figure 6. Quantitative tests to assess the extrudability, filament formation, and shape fidelity of bioink prior to the printing process. (A) Rheological data can be acquired for a specific ink, providing key information on properties necessary to extrude cohesive, stackable filaments. (Ai) Yield stress measurements correlate with the flow initiation step, (Aii) whereas shear-thinning properties of a bioink permit facile extrusion. (Aiii) Depending on the extrusion pressure and the polymer viscosity, droplet, or filament formation can occur at the nozzle. (Aiv) Bioinks able to form filaments and also show a rapid shear recovery after extrusion, can be used for printing and stacking multilayer constructs with improved shape fidelity.[144] (B) Uniformity of each extruded filament and thus its shape fidelity compared to the intended design (typically a cylindrical, smooth filament) can be assessed via image analysis and correlates with the ability of a viscoelastic bioink to absorb and disperse energy, as quantified by the loss tangent (tan (δ)). Higher values of the loss tangent were shown to correlate with better filament uniformity.[162] (C) Printed filaments can experience different deformations, given their limited mechanical properties, under the action of different forces, including gravity and surface tension.[78] (Ci) Printing a bioink filament on top of an array of pillar placed at increasing distances offers a simple and quantifiable way to assess sagging of support-free structures due to gravity (and, in absence of postprinting cross-linking to the viscoelastic properties of the hydrogel ink), as estimated via assessing the deflection angle θ. (Cii) Adjacent filaments in a filament fusion test (deposited in a meandering pattern at increasing filament distances, f_d) can merge due to the surface tension between the bioink and the collector substrate, as well as between each layer of a bioink. Inks with lower yield stress tend to have longer fused segment length (f_s) even at higher f_d, causing a loss of resolution in the x–y plane. Schematics based on proposals from Paxton et al.[144] (A), Gao et al. 2018[162] (B), and Ribeiro et al. 2017[78] (C).

The main limitation of the use of this model is, however, that it can only be applied to a range of shear rates between 10 and 10^4 1/s.[144] Further, it assumes that the fluid is steady and linear at medium shear rate and does not account for wall slipping, e.g., reduced viscosity near needle wall.[144] A model that take into account low shear rate regions is the Herschel–Bulkley model (eq 4), which relates the shear stress (τ) to the yield stress (τ_0), shear rate, and the shear-thinning parameters of the power law (k and n):

$$\tau = \tau_0 + k\gamma^n \tag{4}$$

The Herschel–Bulkley model is quite useful, because it includes both the yield stress and shear response and even considers wall slipping within the needle.[100,135,166] Although such theoretical models can be implemented as an in silico tool to gain insight in the potential printability of a material, experimental validation is still needed, as the models are based on simplifications and assumptions. It should also be noted that the above predictive models are particularly relevant for extrusion-based printing. In lithography-based bioprinting, rheological requirements are vastly different. In fact, the bioink usually consists of a low viscosity (usually 0.25–10 Pa·s[167]) photo-cross-linkable hydrogel precursor.[20] The kinetics of the photochemical cross-linking, the diffusivity of the generated reactive species, and the presence of inhibitors and optical properties of the resin are the major determinants of shape fidelity, and these will be discussed in more detail in section 5.2.

4.2. Extrudability and Filament Formation

The evaluation of fiber formation and stacking ability is a first important step in assessing and potentially predicting shape fidelity in extrusion-based printing. First, the flow of the bioink needs to be initiated upon extrusion, which occurs when the extrusion pressure exceeds the yield stress of the ink. To evaluate extrudability, the force needed to extrude the bioink at a constant speed can be measured.[160,164−166] Homogenous inks will result in constant extrusion forces, often leading to the looked-for continuous extrusion, while particle or aggregate induced ink inhomogeneity and associated fluctuation of extrusion force over time can reduce consistency of the deposited filaments.[168]

Further, visual screenings of whether a droplet or a continuous and linear filament are formed upon extrusion into the air have often been proposed as initial steps to identify optimal printer settings.[42,46,144,169,170] This ability to form a filament and display uniform extrusion is directly associated with the material's shear-thinning and rapid shear recovery behavior (Figure 6Ai–iv).[144]

Once a continuous filament can be extruded, the uniformity and thus shape fidelity of deposited single lines can be investigated.[160,162,171] A wavy structure of the filament may clearly require further optimization of the printer settings. The ability to extrude a uniform linear filament is affected by the

https://dx.doi.org/10.1021/acs.chemrev.0c00084
Chem. Rev. 2020, 120, 11028−11055

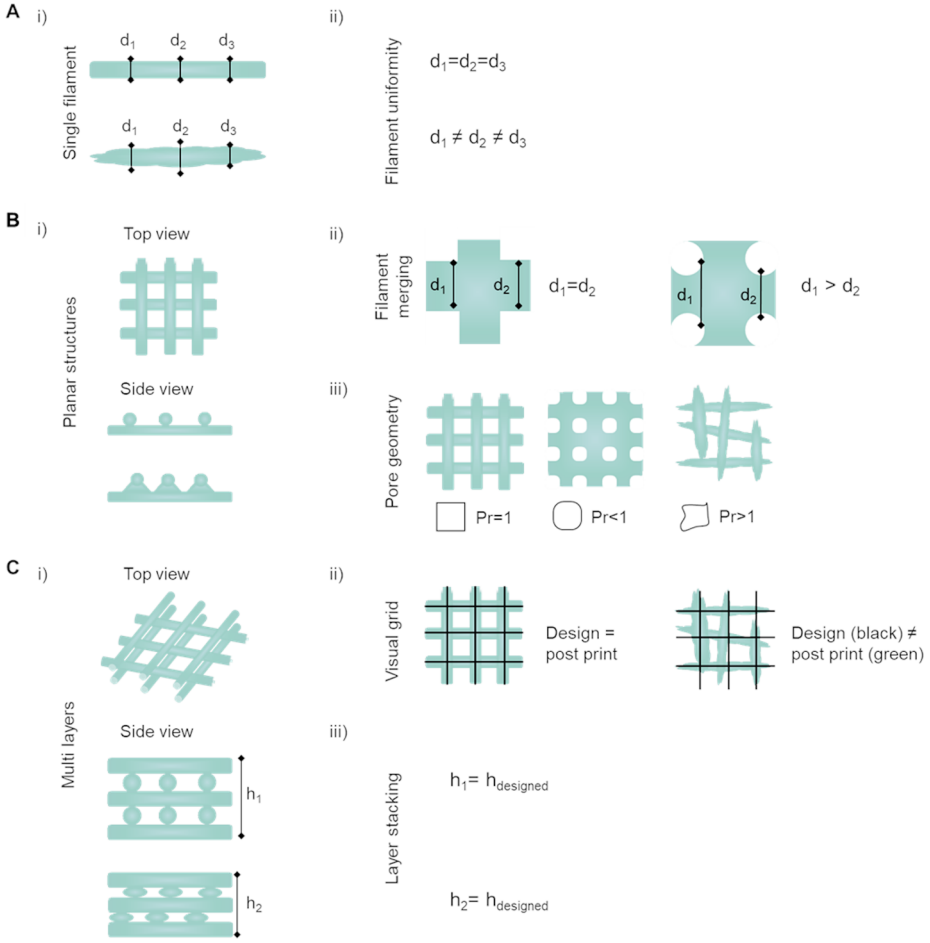

Figure 7. Quantitative tests to assess the shape fidelity of a bioink during printing and postfabrication. (Ai) Single filaments are evaluated on their (Aii) homogeneity based on the fiber diameter (d_1, d_2, and d_3), with identical diameters characterizing a homogeneous filament.[163,178] (Bi) Top and side view of 2D planar structures, meaning constructs that predominantly extend along two directions which are significantly wider than the height of the constructs which are typically composed of 1−2 layers. Planar structures being evaluated on (Bii) filament diameter and merging with focus on the intersection/overlay of two filaments and (Biii) transversal pore geometry with optimal rectangular pore shape for ideal filament stacking (printability index $P_r = 1$).[46,163] (Ci) Top and side view of multilayered constructs illustrating circularity of filaments.[46,105,140] (Cii) Visual grid as indicator how close the printed structure (green lines) match with the computer designed shape (black lines) post printing.[105] (Ciii) Layer stacking indicating the shape retention of circular filaments in multilayered constructs is analyzed by comparing the height of the computer designed sample to the height (h_1 and h_2).[162,163] Schematics based on proposals from Soltan et al. 2019, Wang et al. 2018[163,178] (A); Ouyang et al. 2016, Soltan et al. 2019[46,163] (B); and Petta el al. 2018, Gao et al. 2018, and Soltan et al. 2019[105,162,163] (C).

printing pressure and the nozzle speed, but also by the nozzle offset,[17] e.g., the distance between the tip of the nozzle and the building platform.[37,94,98−100] These process parameters which are dependent on the nozzle diameter and geometry can greatly vary between different bioinks.

Given their limited elastic properties, viscoelasticity, and propensity to undergo structural deformations, printed filaments can display creep and collapse exemplified by merging of the filaments or layers. This can occur when the bioink does not stop flowing immediately after leaving the nozzle, or if the yield stress (or storage modulus) is too low to counter forces, such as gravity and surface tension.[78,172,173]

For achieving a high shape fidelity, the ability to print structures with transversal porosity is important and hence preventing filament collapse along the axial direction due to the effect of gravity is imperative, especially when a filament is spanning over a large gap between underlying supporting structures, or even when overhangs are to be produced (Figure 6Ci). The potential of a given bioink to counter gravity can be quantitatively evaluated through printing a filament over a pillar array, bridging a gap at increasing distance, e.g., as previously reported with gap sizes ranging between 1−12 mm and measuring the angle of deflection[78,172] or the area below the filament.[42,174] The angle of deflection θ, expressed as a function of the gap distance, is a measure of the deformation suffered by the filaments due to the discrepancy between the gravitational force given by the filament's own weight, and inertia measured by yield stress and storage modulus of the ink. In particular, yield stress was suggested as predictor of potential filament deformation as increasing values for this parameter correlated with lower deflection angle values.[78] A simplified version of the filament collapse test has been applied also for bioinks with low elastic modulus and limited structural integrity, which are unable to span over large gaps across pillars and simply break rather than undergo sagging. In this setting, multiple filaments are printed from the same ink, and the number of gaps that can be covered without fracturing the filament were calculated.[175]

Besides gravity-driven deformations, adjacent filaments printed in a same layer can fuse due to the time-dependent

https://dx.doi.org/10.1021/acs.chemrev.0c00084
Chem. Rev. 2020, 120, 11028−11055

flow (prior to stabilization via cross-linking), as well as due to spreading onto the underlying layer (or printing collector, if it is the first layer) caused by surface tension. A straightforward test to analyze such filament fusion was proposed printing parallel structures[176] or filaments with a stepwise narrowing of the filament spacing (Figure 6Cii).[78] In such a meandering pattern, the fused portion of the filament propagates from the corner and increases (up to cause a complete fusion of the filaments, closing the intrafilament space) for decreasing filament spacing and for bioinks with decreasing yield stress.[78] This test is indicative of the capacity of printing fine details like small pores with sharp angles.

Taken together, for proper assessment of the bioinks, all events and parameters that determine the deformation of printed inks need to be considered in relation to the viscoelastic behavior of the material of interest.[177] While yield stress was proposed as a relatively straightforward indicator of the resistance of a given bioink to sagging and fusion, a complete modeling and understanding of these phenomena should not overlook the impact of time-dependent effects. For example, filament collapse or fusion due to lack of yield stress and low viscosity inks should also be carefully considered as these may occur on a time scale short enough to introduce artifacts in the print.

4.3. Shape Fidelity in Planar Structures

Besides the filament formation, filament homogeneity and uniformity are also important aspects in order to generate planar structures. Planar structures are constructs that predominantly extend along two directions (x and y plane), which are significantly wider than the height of the construct. This typically translates to structures composed of 1−2 layers as used in more qualitative and quantitative shape fidelity tests reported in the literature. For example, filament diameter can be measured on images of the filament at different locations (Figure 7A)[58,62,163,168,171,178] or indirectly calculated by measuring distance between filaments.[179] Normalization of the diameter measured on the printed filament to the needle diameter results in the spreading ratio.[51] Further, the filament diameter at the intersection of two filaments[180] can be used as an indicator of how well these are stacked and how the filaments may deform due to surface tension. Fusion is accompanied by an increase in diameter in x−y plane, as the filament relaxes and spreads onto the underlying layer (Figure 6Bii).[178] Beside filament width, the height of printed filament has been examined in image-based analysis.[134,181,182] Measuring the filament width (x−y plane) and thickness (z-axis) across multiple points along the length of a given filament or planar structure which are then compared to the original dimensions of the computer-aided design (CAD) file at the same points (Figure 7Cii) are also referred to as geometrical accuracy.[178,183] Filament diameter and height are linked to printing parameters, such as feed rate,[134,181,182] nozzle diameter,[184−186] pressure,[42,182,185] nozzle height,[134,181] and nozzle speed.[42]

Poor or slow stabilization of the ink after dispensing, as well as fusion of adjacent filaments are in fact marked by the collapse of the filament circularity.[78,174] Semiquantitative evaluation, based on the circularity of printed filaments and shape fidelity of the pore, was recently introduced.[46,140] Using this approach, a printability index (P_r) which is based on the perimeter and area of the pore can be easily derived (Figure 6Biii). An ideal axial porosity in a 0−90° laydown pattern should thus display a squared (or rectangular, depending on the designed strand-to-strand distances) profile in the x−y plane. In this case, high geometric accuracy would result in a printability index of $P_r = 1$ (square shape transversal pore geometry), while $P_r < 1$ and $P_r > 1$ correspond to a more round or irregular shaped transversal geometry, respectively.[42,46,170,187−189] Thus, the measurement of pore circularity and the deviation from an ideal square, can provide an estimation of the shape fidelity in the x−y plane.[46] Low viscosity and nonoptimal gelation conditions are some of the underlying causes for these deviations, e.g., the merging of filaments and the resulting low shape fidelity.[46,144] Thus, approaches, such as postprinting light cross-linking (e.g., visible or UV light), should be considered to increase filament stability after extrusion. Recently, a combined evaluation on printability and rheological properties was introduced by correlating the filament width deviation from the needle diameter to G' or gelation time, or calculating the deviation from the square area of the printed construct (1 or 3 layers) varying the pH for gelation of collagen bioinks.[190]

4.4. Shape Fidelity in Multilayered Structures

Once reproducible control over the deposition of filaments in a single layer is achieved, the shape fidelity of constructs based on multiple layers should be evaluated. Important parameters that have been proposed for this assessment are the geometric accuracy, layer stacking, and structural integrity. In addition to geometrical accuracy described in the previous section, the measurement of the maximal height reached for printing a defined geometry indicates quality of layer stacking in a multilayered setup, often described as critical height.[135,162,191]

Analysis of shape fidelity and integrity index both rely on the calculated percentage of construct dimensions postprinting relative to the theoretical designed ones. Indices <1 indicate filament merging and/or collapse, whereas indices of 1 refer to high shape fidelity and optimal layer stacking (Figure 7Ciii).[55,62,105,162,163,188] To assess shape fidelity and reproducibility and to identify defects or artifacts within a construct postprinting, 3D computed tomography (CT) imaging has been proposed. Constructs can be visualized by CT, even though due to the high water content, inks made only of hydrogels show limited CT contrast.[192] Nevertheless, using decreased beam intensity and focusing on the lower range of the gray values, morphometric analysis of micro-CT scans of hydrogel-based constructs is feasible (Figure 8A).[105]

An advantage is that this technology is well-established in the field of material science and that associated morphometric tools and software are already available.[193−196] Further, CT can also reveal additional defects in printed structures, such as air bubbles within filaments. However, as this technology relies on the use of X-ray, it is not optimal for the analysis of cell-laden constructs, except for end-point measurements.

Optical coherence tomography (OCT) is an additional method that allows for 3D visualization of water-rich samples, such as hydrogels (Figure 8B). In fact, OCT imaging provides a 3D volumetric view of the inner microstructure of a translucent and opaque construct.[197−200] It allows quantitative assessment of morphological parameters, including pore size, filament size, porosity, surface area, and pore volume with high contrast between hydrogel and pores and has been proposed as a real-time monitoring technique with high resolution (1−10 μm) and signal acquisition speed (25 frames/s).[178,192] The advantage of OCT imaging compared to fluorescence or

https://dx.doi.org/10.1021/acs.chemrev.0c00084
Chem. Rev. 2020, 120, 11028−11055

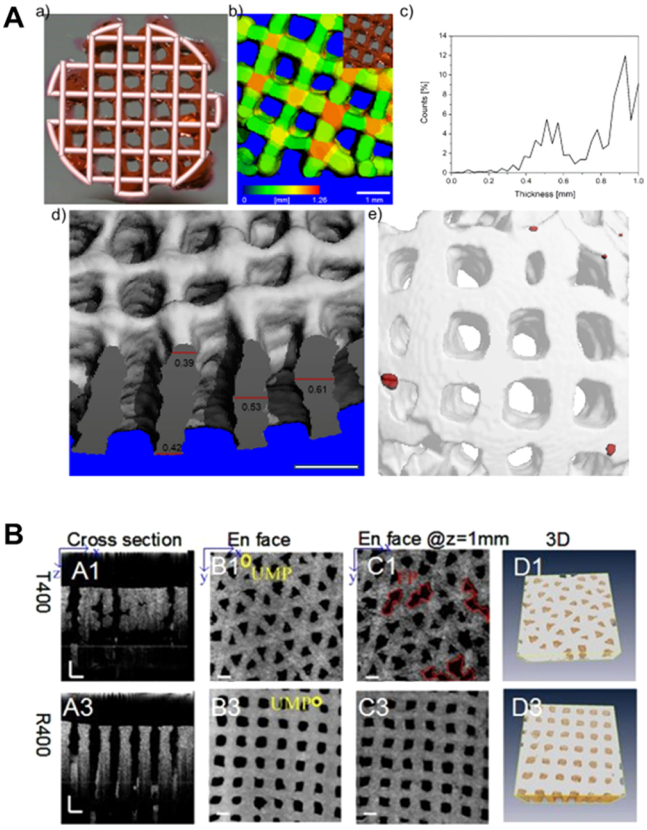

Figure 8. Use of CT and OCT for visualization of filaments and pore structure in printed hydrogels for the evaluation of shape fidelity. (A) Use of micro-CT to assess shape fidelity of 3D printed HA-based hydrogel: (a) Optical image of a 3D printed lattice grid overlapped with its 3D CAD model; (b) micro-CT 3D reconstruction of the printed construct, where the color represents the thickness; (c) Strut thickness distribution in the 3D reconstruction; (d) micro-CT cross-section of a 3D printed construct of multiple layers illustrating overlaying accuracy; (e) 3D reconstruction image showing air pockets in red. Scale bars 1 mm. (A). Reproduced with permission from ref 105. Copyright 2018 American Chemical Society. (B) Optical coherence tomography (OCT) imaging of gelatin/alginate hydrogel with different architectures illustrating (A1, 3) the cross-section; (B1, 3) surface; (C1, 3) hydrogel at 1 mm depth; and (D1, 3) 3D observation of hydrogel matrix. Scale bars 500 μm, UMP: undefined micropores. (B) Adapted with permission from ref 192. Copyright 2106 The Optical Society.

scanning laser confocal microscopy is the increased penetration depth of up to 1000 μm, while fluorescence microscopy only allows the analysis of the construct surface, and the penetration depth of confocal microscopy is limited to 300 μm.[201,202] Importantly, OCT is compatible with cell-laden hydrogel structures, is noninvasive and uses only a low exposure dose with a swept-source laser (scanning rate, 50 Hz; spectrum, 1310 ± 60 nm).[178] Moreover, the outcome can be directly compared with the original CAD file, and thus can provide immediate input for the improvement of shape fidelity of the printed constructs.

4.5. Noninvasive and On-the-Fly Monitoring

The approaches described above provide an important insight into the printability and shape fidelity of filaments, layers, and 3D constructs. However, they do not allow for the in-line monitoring of the progress of a print neither to apply changes in the printing parameters while printing, which could be beneficial to fully automate the bioprinting workflow. Thus, in an ideal set up, shape fidelity and printing quality should be monitored in real-time and in a nondestructive manner. Such an approach would also require a feedback loop, using the acquired information on geometrical parameters detected during printing as input for adjusting, e.g., the extrusion rate or the printhead velocity.

Until now, OCT-based real-time monitoring is not yet available. However, it could provide a future opportunity for noninvasive iterative feedback control when integrated into a bioprinter system. Although such hardware is not available yet, algorithms to provide feedback for optimizing the printing process, based on OCT analysis of as-printed sample constructs have already been proposed.[178]

Further advances can derive from implementing new machine learning processes, which have so far been applied to optimize the printing resolution of silicone-based elastomers.[212] Specifically, a set of shape fidelity scores estimating layer fusion, stringiness (adhesion of layers), and undesired pore infill caused by collapse of the printed materials, were used as inputs for machine learning methods that had as output estimated optimal printing parameters. Likewise, machine learning algorithms have been recently investigated to predict the printing window of collagen-based bioinks, starting from rheological data.[213] The combination of advanced imaging hardware and shape fidelity predictive software, could pave the way for automated on-the-fly optimization of bioprinting accuracy.

4.6. Approaches to Overcome Forces Impacting Shape Fidelity

The main sources of printing artifacts, i.e., the deformation of generated bioink-based 3D structures resulting in a deviation from the intended design, and thus in a decreased shape fidelity, are gravity, surface tension, and time dependent flow behavior of the bioink prior to chemical or physical stabilization. Such forces play a critical role in extrusion-based technologies and the introduction of new strategies to counteract them has been a primary motivation in recent research efforts in the field of bioprinting. As many of these forces directly interplay with properties that are intrinsic to the physicochemical properties of the bioink, one approach aims at refining the design of the bioink itself, so that its rheological behavior and properties can prevent or minimize such deformations (e.g., a storage modulus and yield stress that are sufficiently high to prevent buckling of suspended filaments). Proposed approaches go from adding rheological modifiers and viscosity enhancers (in the form of micro- and nanoparticles,[112,187,214−217] nanofibrous elements,[98,218,219] nanoclay,[220−222] or blends of different biomaterials[223−226]), design of advanced chemistries to provide shear-thinning and rapid and reversible stiffening of the extruded filaments (e.g., host−guest chemistry and reversible bonds[227]), as well as the formation of colloidal inks or gels formed by slurries of preformed microgels[103,104] capable of flow under applied shear forces. While these approaches introduce a direct modification of the inks, either in terms of chemical composition or of the physical form in which the ink is presented (e.g., as microparticles or as a solution), other promising approaches aim at modifying the surrounding environment in which the printing process occurs, or the printing hardware itself to optimize the timing in which stabilization and cross-linking chemical reactions occur within an ink. These approaches, in

https://dx.doi.org/10.1021/acs.chemrev.0c00084
Chem. Rev. 2020, 120, 11028−11055

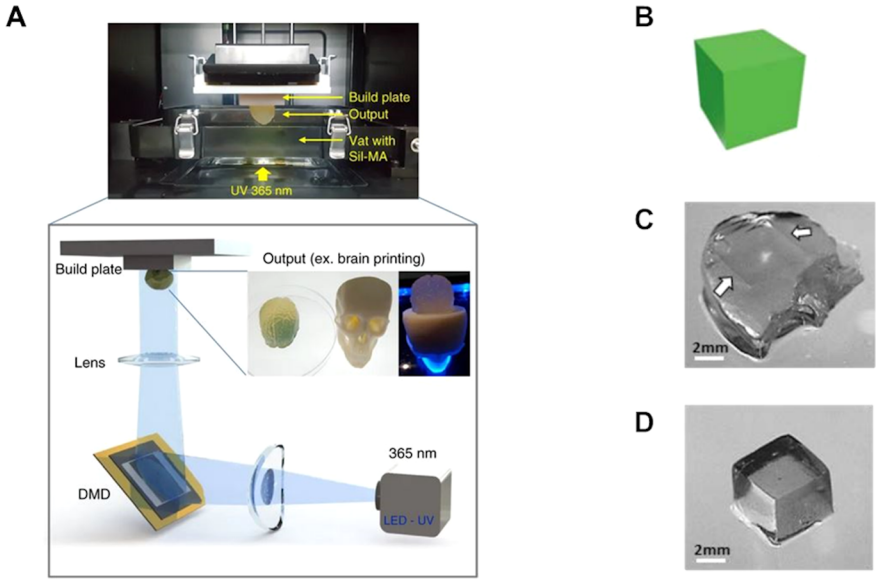

Figure 9. Schematic illustration of DLP printing and the effect of overcuring. (A) Schematics of a DLP printing approach, with a particular example using silk derived bioresins. (A) Adapted with permission from ref 263. Copyright 2018 Springer Nature under CC BY 4.0 (https://creativecommons.org/licenses/by/4.0/). (B) Example of improved printing resolution via addition of a biocompatible food dye as photo absorber to a PVA-MA bioink. CAD design of a cube, (C) overcured print, and (D) printed cube with sharp edges, from the photo absorber-laden bioink. (B–D) Adapted with permission from ref 247. Copyright 2018 IOP publishing under CC BY-NC-ND 3.0 (https://creativecommons.org/licenses/by-nc-nd/3.0/).

particular, have the potential to enable the utilization of bioinks poorly printable with conventional methods, but that could readily provide a biomimetic environment for cells to thrive. Like in conventional 3D printing, support materials, in the form of stiff hydrogels,[228] ceramics,[33,176,229] or thermoplastic polymers,[31,33,55] can be included to provide long-lasting structural fidelity to constructs based on bioinks displaying low mechanical properties. Likewise, sacrificial materials e.g., based on thermosensitive hydrogels (e.g., gelatin[230−232] or poloxamers[101,233,234]) or alginate,[235,236] can be used to print temporary supports.[234] The effect of gravity on printed filaments, as well as that of deformation due to time-dependent flow prior to cross-linking can be countered by printing within an environment providing buoyancy or direct support to the bioink, for instance via suspended printing into support bath, made of shear-thinning polymers, fluidized gels, or granular media, as reported for example with the approach termed freeform reversible embedding of suspended hydrogels, or FRESH.[4,104,237−239] In terms of techniques providing accurate control over the cross-linking kinetics and its timing within the different stages of the bioprinting process, coaxial,[139,240−242] or microfluidic circuit-coupled nozzles,[243] as well as light permeable nozzles[208,244] have been designed to promote cross-linking of low viscosity inks at the moment of extrusion, thus reinforcing the resistance of such hydrogels against sources of deformation.

The above-mentioned innovative approaches have the potential to substantially increase the range of suitable bioinks for printing, successfully improving shape fidelity even when using hydrogels, which would display poor printability when extruded in standard ambient conditions. Further refinement of these technologies, as well as new future directions in biomaterials design and engineering are expected to remain major research topics in biofabrication in the near future. Given the importance of these aspect, these technologies have also already been extensively covered in other valuable reviews.[92,126,237]

5. IMPLICATIONS FOR LITHOGRAPHY-BASED PRINTING TECHNOLOGIES

Alongside the efforts to improve shape fidelity and to overcome the difficulty of extruding low viscosity materials into cohesive structures, 3D printing technologies which have operating principles that are nozzle-free and do not require filament formation are acquiring increasing relevance within the field of biofabrication. Specifically, lithography-based printing technologies, derived from traditional vat polymerization, are of particular interest due to their superior resolution compared to extrusion-based techniques and freedom of fabrication of free-form, complex 3D structures.[14] Although often generically referred to as stereolithography (SLA), a term that specifically defines the printing process driven by laser scanning of a photoreactive resin in vat,[245] many different lithography printing technologies exist, including DLP printing, and multiphoton polymerization (MPP) printing, and all of them have been used for cell printing in biofabrication. For this family of techniques, many of the rheological analyses and quantitative tests based on filament structures described in sections 3 and 4 provide little information. Still, postfabrication shape fidelity remains an important aspect also in the context of lithographic techniques, especially when using cell-laden hydrogels that could display low mechanical properties. In this section, the basic working principles of lithographic techniques and the phenomena that could impair shape fidelity in light-based technologies are described together with the analytical tests to assess shape fidelity.

https://dx.doi.org/10.1021/acs.chemrev.0c00084
Chem. Rev. 2020, 120, 11028−11055

5.1. Working Principles of Lithography-Based Bioprinting Technologies

A common factor in lithographic printing methods lies in the inks used, often termed resins, which consist of photo-cross-linkable prepolymer mixtures, loaded with a photoinitiator. In analogy to this concept, bioinks for lithographic bioprinting are sometimes termed bioresins.

In these processes, the bioresins are generally stored in a vat or reservoir and are selectively exposed to light to induce gelation of the ink in a spatially controlled fashion to generate a 3D object. The main differences across the various lithography-based technologies is the exact mechanism of irradiation of the photopolymer in the vat. SLA and DLP printing, respectively, focus a laser spot or a pattern of light drawn by a digital micromirror device (DMD) on a thin layer of the prepolymer (typically 25 μm[12] to 75 μm[246,247]). The process is repeated in a layer-by-layer fashion, as the cross-linked part is either lifted from (bottom-up) or sunken into (top-down) the vat through the automated movement of a building platform, on which the printed construct is attached. In bottom-up set-ups, a new layer of resin flows in between the optical window at the bottom of the vat and the build platform, whereas in top-down printers, new resin is automatically added on top of the printed construct. Conventional SLA allows for higher resolution (<30 μm[248]) but is associated with longer printing times (delivery rate $\approx$ 10 mm^3 min^{-1}[5]), due to the scanning of the laser across each layer. In DLP (Figure 9), on the other hand, every pixel in each layer is projected in parallel onto the resin, allowing for faster fabrication rates (delivery rate $\approx$ 20 mm^3 min^{-1}[5,248,249]) in lithography-based bioprinting.[167] An advantage of light-based systems over extrusion approaches is the possibility to print structures directly into a volume and therefore even add and remove, via photo-cross-linking or photodegradation,[250] elements from an inner part of construct without altering the bulk of printed structure. While this remains challenging with conventional light projection or laser scanning, like DLP and SLA, in-volume printing, and conversely etching, can be achieved with new single-photon technologies based on tomographic principles,[11] as well as with technologies that rely on multiphoton absorption.

MPP is a typical example of this potential, also showing currently the highest resolution in terms of bioprinting technologies, resolving features in the nanometer range.[251] In two-photon polymerization process, the most common among multiphoton-based printing, a volume of the resin is irradiated with a laser of wavelength typically in the infrared region of the spectrum, which is normally not able to excite the photoinitiator (which is often chosen among those absorbing in the 365−450 nm range[167,248]). Only in the spot where the light is focused, a two (and per extension multi) photon absorption event can occur, providing enough energy to trigger local photo-cross-linking in the sole focal spot. Hence, by scanning a volume of resin, 3D objects can be generated. Among single-photon technologies, recently, the concept of volumetric bioprinting (VBP) using visible light tomographic projection has been introduced, making it possible to print features inside any desired region of a volume of a photo polymer.[11] In this technology, the workflow is inspired by that of CT in reverse. Briefly, applying a tomographic algorithm (e.g., Radon transform), filtered back projections at different view angles, are obtained from a 3D CAD design. These are then rapidly casted using visible laser light and a digital micromirror device onto a rotating volume of photopolymer. Differently from layer-by-layer manufacturing, the whole volume of photopolymer is exposed at once. The convergence of the light projections generates a 3D optical field of voxels, in which the irradiation dosage is above the cross-linking threshold of the bioresin. Such a mechanism makes it possible to sculpt the (cell-laden) hydrogel into a 3D construct at once in a time frame of less than 30 s.[11]

5.2. Printability and Shape Fidelity in Lithographic Printing

Because the printing process is entirely based on spatially controlled light irradiation, photo-cross-linkable materials mixed with appropriate photoinitiators are necessary, and most of the requirements for high-shape fidelity printing revolve around the control over the photo-cross-linking reaction. Second, a wide array of high and low-viscosity prepolymer solutions (typically in the range 0.25−10 Pa·s[252]) can be easily processed, without the need to exhibit shear-thinning behavior.[253] In particular, low viscosity inks are beneficial in SLA and DLP printing, as they can easily flow under a lifted printed part in bottom-up approaches (or be placed homogeneously on top of the construct in a top-down equipment). Such low viscosity hydrogel precursors would facilitate removal of the unreacted bioink from pores or narrow negative features within a print, therefore improving the resolution of the process and reducing printing artifacts. Currently, several hydrogel systems commonly used in biofabrication have been adapted for lithographic printing. These include hydrogel platforms based on chain-growth polymerization, such as acryloyl-modified poly(vinyl alcohol),[247] PEG,[117,254−256] PEG−cellulose nanocomposites,[257] poly(trimethylene carbonate)-poly(ethylene glycol)-poly(trimethylene carbonate),[258] gelatin,[255,259−261] gelatin−polyaniline,[262] alginate,[47] silk fibroin,[263] pullulan,[264] or based on thiol−ene step-growth polymerization systems, e.g., gelatin−norbornene[265] and allylated gelatin[253] that can be used in combination with several UV[254] and visible light photoinitiators.[247,255] Additionally, besides using photo-cross-linking, noncovalently cross-linked alginate hydrogels have also been processed with DLP, via the incorporation of photoacid moieties in the ink formulation, to tune the rate of ionic bonds formation between calcium cations and the anionic alginate chains.[266]

Shape fidelity is mainly dependent on (i) printing resolution and (ii) efficiency of cross-linking and structural stability postprinting. For lithographic and vat polymerization techniques, the theoretical resolution depends on the printing hardware (minimum feature that the light pattern can resolve), and it generally ranges from <5 μm in SLA,[246] VBP,[11] and DLP[247] processes to tens of nanometers for MPP.[267] The minimum volume unit, or voxel, that can be resolved in the irradiation-cross-linking process, determines the topography and roughness profile of the surfaces within the printed part. However, achieving a photopolymerization that is perfectly confined within the irradiated spot is a major challenge. The resolution is effectively altered by the absorbance of the bioink mixture at the irradiation wavelength by the scattering of light and by the diffusion of the reactive species generated from the irradiation of the photoinitiators within the bioink mixture. The combination of these factors could induce undesired photopolymerization in the proximity of the illuminated spot, lowering the printing resolution in the x, y plane (perpendicular to the direction of irradiation) and in the z-

https://dx.doi.org/10.1021/acs.chemrev.0c00084
Chem. Rev. 2020, 120, 11028−11055

direction (parallel to the irradiation path). Ideally, inks that quickly cross-link depleting the generated radicals and display high light absorption at the irradiation wavelength are preferred. High absorption is particularly important in DLP and SLA processes to control the resolution in the *z*-direction, which is greatly affected by the curing depth, defined as the thickness of the gelled ink layer as a function of the irradiation dosage.[268] As for resins for traditional lithographic printing, each given bioink formulation can be defined by a minimum irradiation dosage above which gelation occurs, which is a function of the type of material, initiator, and concentration of dissolved inhibiting species (e.g., oxygen for free-radical polymerization) as well as by its curing depth.[248] Ideally, the curing depth of a given ink should be higher than the layer height selected for the process to ensure gelation and integration at the interface between two consecutive layers. At the same time, light penetration beyond the designed layer thickness could cause unwanted polymerization of parts that were initially designed to remain uncured (e.g., pores), introducing artifacts in the constructs. For this reason, accurate control over the curing depth is a major requirement in DLP and SLA printing. While it is possible to reduce light penetration depth simply through control over the printing parameters, namely irradiation dosage and wavelength,[263] the bioink mixture can also be tuned via the addition of photo absorbers. These are nonreactive molecules that exhibit absorbance at the wavelength of the irradiation source and therefore compete with the photoinitiators, limiting both light scattering and overcuring across printed layers (Figure 9C). Photo absorbers are particularly useful for improving control over cross-linking for bioprinting purposes, as hydrogels for cell culture and biofabrication, unlike most conventional photo resins, are often transparent in the visible and near-visible UV range. Recent reports have identified biocompatible photo absorbers, including ponceau red,[247] nanohydroxyapatite,[269] and melanin nanoparticles.[270] Conversely, photo absorbers are generally not required in MMP technologies, which are less affected by light scattering and bleeding across different layers, causing unwanted polymerization. Shape fidelity and resolution in MPP is prevalently dependent on the point spread function of the multiphoton event, which can be controlled by selecting the design of the laser irradiation and focusing system, and on the reactivity of the photoinitiator, thus making the selection of the initiator an important step to modulate resolution.[271]

The presence of cells within the hydrogel precursor solution can also influence the photo cross-linking reaction and can impact on the mechanical properties of the hydrogel resin,[272] which in turn can result in decreased shape fidelity of the final constructs. However, to date, the effect of embedded cells on shape fidelity of bioresins for lithographic printing has received only little attention and additional research is required. Sedimentation of cells suspended in the resins is also an important aspect, in particular, when long printing times or low viscosity hydrogel precursors are involved. Cell sedimentation can be prevented either through supplementation of the bioresin formulation with viscosity enhancers[117] or by applying gentle movement of the build platform between the printing of each layer.[247] Moreover, in contrast to extrusion printing, in vat polymerization technologies, the unreacted, leftover bioresin volume needs to be washed away and removed. Although this can potentially be reused for subsequent prints, it generally leads to a significant loss of (valuable) cells and materials.

On the other hand, because the part is immersed in a (bio)resin volume during printing, the unreacted polymer supports buoyancy to the cross-linked gel, facilitating the resolution of highly porous structures and overhanging architectures, even when little to no support structures are printed. However, retention of the imposed shape postprinting can be challenging depending on the mechanical properties of used hydrogels after gelation. The same considerations on hydrogels for extrusion-based printing apply, and soft, loosely cross-linked networks are preferred for cells to thrive.[21] These, however, may not be able to withstand their own weight, depending on the hydrogel used, and printed porous architectures may collapse when outside a watery environment. Moreover, such unstable constructs may have limited potential in load bearing applications but may be beneficial when deformable, foldable gels are required, for instance, for minimally invasive implantation in vivo (e.g., through catheters or arthroscopic probes),[273] provided their intended shape can be recovered. Co-printing with stiff support structures, a common strategy in extrusion-based technologies, can be more challenging with lithographic approaches due to the inherent complication of printing with multiple materials and because most formulations of nonhydrogel forming polymers used as resins carry cytotoxic or harmful compounds.[274] Furthermore, constructs can often be incompletely cross-linked to permit adhesion between consecutive layers. While this can be addressed by further curing via light exposure postprinting, constructs with varying degree of cross-linking can be obtained, tuning their mechanical properties, and therefore structural stability. This aspect needs to be taken into account, as it directly influences the tendency of the printed material to swell in aqueous media, which would in turn affect the overall shape fidelity.[265] This phenomenon, depending on the curing depth of the ink and its extent of penetration within an already printed layer, has also been exploited to generate scaffolds with gradients of mechanical properties across the *z*-direction.[275] Due to the potential risks in terms of cytocompatibility of unreacted functional groups and poor control over reactivity postprinting, alternative strategies to create gradients, for instance, multimaterial printing, could be preferable.[276] Finally, similarly to most layer-by-layer additive manufacturing technologies, the printed construct tend to exhibit an anisotropic mechanical resistance, as printed parts tend to be weaker when subjected to forces parallel to the printed layers, depending on the adhesion strength between each layer. Moreover, layerless biofabrication methods, like VBP generate materials with smooth surface features and continuous structures, and therefore do not display such mechanically weak junctions throughout the print.[11] In addition, in the field of lithographic printing of bioinks, the development of fast printing approaches with higher lateral resolution has been demonstrated via the continuous liquid interface production printing.[277] This variation of DLP and SLA technology takes advantage of the use of inks based on acryloyl chemistry, in which chain polymerization reaction can be inhibited by the presence of oxygen species. Introducing an oxygen permeable membrane between the vat and the optical window used for irradiating the resin permits avoiding cross-linking at the bottom of the material reservoir, and therefore detaching the printed part rapidly, with minimal forces, enabling a much rapid, nearly continuous printing process.[278] With such an approach, the integration between consecutive layers is facilitated, giving rise to structure with superior mechanical

https://dx.doi.org/10.1021/acs.chemrev.0c00084
Chem. Rev. 2020, 120, 11028−11055

stability compared to conventional layer-by-layer additive manufacturing.[277] While oxygen inhibition can be the cause for inadequate cross-linking and hampering shape fidelity, spatially controlled presence of oxygen species within a printed geometry have been purposely used to create hydrogel structures with local differences in mechanical stiffness. For instance, PEG dimethacrylate constructs with vertically oriented pillars, displaying different elastic modulus were printed, creating gels that can bend easily in the areas laden with soft pillars, which can have application as hydrogel-based actuators.[279] Overall, tuning all the above-mentioned parameters is paramount to improve shape fidelity in lithographic approaches.

Postfabrication shape fidelity assessment can be complex with conventional microscopy techniques, as lithographic approaches are often used to generate convoluted constructs, which have geometrical features difficult to image. 3D imaging methods, such as CT, can however aid in the assessment of volumetric shaped fidelity and mismatch between CAD designs and finalized prints. Finally, technologies able to detect printing defects on-the-fly (and thus possibly providing feedback to correct printing defects), which are now appearing in the field of extrusion printing (e.g., live scanning of the printed parts), could be readily applied to lithographic techniques.

6. CONCLUSION AND OUTLOOK

In the field of biofabrication, cell-friendly hydrogels and soft materials remain among the most studied and promising scaffolding and structural components in many bioink formulations. Differently from conventional engineering materials, such as thermoplastic polymers, metals and ceramics used in the AM industry, the limited structural stability of hydrogels, high water content, and viscoelasticity pose a major challenge toward the bioprinting of constructs which display accurate and highly porous geometries, as often sought in regenerative medicine. The challenge of achieving structures with high shape fidelity to closely mimic native tissues has been a major focus for many researchers,[38,280−282] and the field is now looking toward how such architectural control can be exploited to capture the functionality of biological tissues.[92]

Although there is consensus on the importance to accurately control high-resolution features in 3D bioprinted tissues, to date, "printability" remains a widely used yet poorly defined term, often employed to address, for example, extrudability, filament formation (in extrusion printing), and shape fidelity and retention over time. Notably, most reports in the literature still describe qualitative screenings of printed structures from macroscopic imaging. This often provides subjective observations and does not aid to reproducibly assess how a given bioink performs in terms of reproducing the CAD models from which the print is originated. Hence, several key aspects, only initially explored in the past years, will need to be embraced in order to improve the design of new bioinks and printing strategies. These include automated analysis systems, quantitative models, and understanding of the constitutive role of rheology in defining printability.

Automation of the fabrication of cell-laden products is a key advance introduced by bioprinting methods, with potential to improve resolution and reproducibility of bioengineered tissues. Yet, bioprinting is still struggling to introduce automated approaches to provide a rapid assessment of printing quality into its toolbox, as well as a feedback loops to the printing hardware to mitigate, mend, and correct potential printing artifacts. Such feedback loops can be envisioned as a powerful tool for moving achievements in the field of biofabrication toward clinical application. Some encouraging steps have been taken related to the coupling of printers with imaging systems for direct monitoring,[178,192] as well as related to using artificial intelligence algorithms that can improve printing resolution.[212] A key challenge in this quest for the automation of fabrication, remains the lack of criteria used to assess what makes a "good" and a "bad" print.

Critically, there is currently no consensus on how to grade printability and, more importantly, on how to objectively and quantitatively describe shape fidelity. Such frameworks should be developed, possibly by a wide, interdisciplinary panel of experts in bioprinting, biomaterials, engineering, polymer physics, and biomedical specialist. Importantly, several authors have independently proposed set of tests that make use of geometrical descriptors to analyze pores and printed struts and how their dimensions relate to the intended CAD designs.[46] A further step in this direction consists in systematically understanding the role of specific rheological properties and parameters on shape fidelity. Quantitative models that attempt to link effects and deformations in as-printed structures, which result in printing artifacts and loss of shape fidelity, to rheological parameters, including storage modulus, loss tangent, yield stress, viscosity, and elastic recovery are being developed. As simple, initial steps in the bioink development process, tests observing the properties of individual filaments can be envisioned and the wider adoption of such simple, reproducible methodology can aid to compare objectively the resilience of a given ink to deformations. Furthermore, such simple analysis can be enriched with the introduction of more complex morphometric assessments (e.g., using CT imaging), which, unlike microscopy and photo/videography, can better visualize and measure how stacked struts form 3D structures with the desired dimension.

To date, attention has been given to filament formation, uniformity upon extrusion, filament collapse, and fusion under gravity and surface tension-driven deformations, phenomena that impair extrudability, as well as resolution and designed porosities in 3D constructs.[78,144,162] These quantitative, objective assessments offer a set of reproducible, simple tests to compare the performance of different bioinks, as well as to improve reproducibility of prints across different laboratories. Moreover, mathematical models based on rheological and printing parameters (needle, pressure, speed) can further aid the refinement of the optimal printing conditions.[144,172] Further development of such in silico models based on rheology and hydrogel physics can lead toward the establishment of predictive algorithms that can provide insight on the shape fidelity that can be achieved with a given bioink. Additionally, it should also be taken into account that postprinting processing could result in deviations from the originally designed shape (e.g., via hydrogel swelling or shrinking[283,284]). This is of particular relevance in approaches termed "4D printing", in which the construct alters its geometry over time, in response to specific stimuli.[285−287]

Overall, a quantitative toolkit to assess printability could be used to generate an initial library of bioinks and their predicted printing resolution and fidelity. Such a database could aid the selection of the most appropriate material for each targeted application, including inks that show poor printability and limited ability to produce 3D patterns. In fact, it should be

https://dx.doi.org/10.1021/acs.chemrev.0c00084
Chem. Rev. 2020, 120, 11028−11055

reminded that, even though architectural organization provides important stimuli for tissue maturation, the required level of resolution to achieve functional bioprinted constructs is still unknown, and that mimicking every facet of a living tissue, down to its single cell resolution, may be unnecessary.[288] If properly instructed by the printed niche and materials, the ability of cells to self-organize could in fact help to bridge the gap toward tissue functionality.[91,289]

Moreover, as the field of biofabrication evolves, new technological solutions are being brought forward. Some of these, instead of focusing on optimizing bioink design, aim to modify the printing environment to permit the high shape fidelity printing of hydrogels and cell suspensions that would otherwise not be able to sustain their own weight, for instance, via suspended bath printing[4] or microfluidic dispensing nozzles.[290] Likewise, despite the major focus in the field has been on extrusion-based bioprinting, lithographic and light-based biofabrication methods, including SLA, MPP, DLP, and VBP, are maturing and it is likely to expect that these techniques will play a more prominent role in the field. In particular, as with these approaches, in contrast to extrusion-based techniques, 3D objects with convoluted biomimetic architectures can be created using low viscosity materials. Although prediction of shape fidelity in these cases will require more refined (*in silico*) models, methods to assess shape fidelity in extrusion printing can easily be transferred to these lithographic and light-based approaches. Overall, significant steps have been taken in the evaluation of extrudability, printability, and shape fidelity in bioprinting, which is also driven by understanding the correlation between shape fidelity, rheological, and physicochemical properties of bioinks. Combining theoretical models and straightforward quantitative tests will in our view be an important and powerful step toward further improving shape fidelity of extrusion-based bioprinted constructs, which will further help toward the generation of functional living tissue models and grafts.

AUTHOR INFORMATION

Corresponding Author

Jos Malda − *Department of Orthopaedics, University Medical Center Utrecht, Utrecht University, 3584 CX Utrecht, The Netherlands; Department of Clinical Sciences, Faculty of Veterinary Medicine, Utrecht University, 3584 CL Utrecht, The Netherlands;* orcid.org/0000-0002-9241-7676; Email: j.malda@umcutrecht.nl

Authors

Andrea Schwab − *AO Research Institute Davos, 7270 Davos Platz, Switzerland;* orcid.org/0000-0002-4576-558X

Riccardo Levato − *Department of Orthopaedics, University Medical Center Utrecht, Utrecht University, 3584 CX Utrecht, The Netherlands; Department of Clinical Sciences, Faculty of Veterinary Medicine, Utrecht University, 3584 CL Utrecht, The Netherlands;* orcid.org/0000-0002-3795-3804

Matteo D'Este − *AO Research Institute Davos, 7270 Davos Platz, Switzerland;* orcid.org/0000-0002-0424-8172

Susanna Piluso − *Department of Orthopaedics, University Medical Center Utrecht, Utrecht University, 3584 CX Utrecht, The Netherlands; Department of Developmental BioEngineering, Technical Medical Centre, University of Twente, 7522 NB Enschede, The Netherlands;* orcid.org/0000-0003-0508-711X

David Eglin − *AO Research Institute Davos, 7270 Davos Platz, Switzerland;* orcid.org/0000-0002-8500-6887

Complete contact information is available at: https://pubs.acs.org/10.1021/acs.chemrev.0c00084

Author Contributions

All authors contributed to the manuscript drafting and have given approval to the final version of the manuscript.

Notes

The authors declare no competing financial interest.

Biographies

Andrea Schwab is postdoctoral researcher in the Regenerative Orthopaedics Program at the AO Research Institute in Davos. She holds a master's degree in technology of functional biomaterials from the Julius Maximilians University Wuerzburg. In 2017, she obtained her Ph.D. (Dr. Rer. /nat.) in Biomedicine from the Graduate School of Life Sciences at the Julius Maximilians University Wuerzburg. Her research focuses on biomaterials, 3D bioprinting, and the interaction and influence of cell laden biomaterials (hydrogels) for application in orthopaedic tissue engineering and regeneration.

Riccardo Levato is assistant professor at the University Medical Center Utrecht. He holds a master's degree in biomedical engineering from the Technical University of Milan, and in 2015 he obtained his Ph.D. in the same field of research from the Institute for Bioengineering of Catalonia and Technical University of Catalonia. His research interests include the development of novel biofabrication strategies and cell-instructive biomaterials for applications in regenerative medicine and tissue biomimicry.

Matteo D'Este earned his Ph.D. in Chemical Sciences at the University of Padova, Italy, with a research project in Theoretical Chemistry. From 2006 until 2011, he worked in pharmaceutical industry in the field of semisynthetic biopolymers and hydrogels. In 2011, he joined the AO Research Institute Davos, Switzerland, where now he is employed as Senior Research Scientist. His research interests include 3D bioprinting, tissue engineering of the musculoskeletal system for fundamental and translational research, musculoskeletal infection, and drug delivery.

Susanna Piluso is postdoctoral researcher at the University Medical Center Utrecht and at the University of Twente. She holds a master's degree in Chemistry and Pharmaceutical Technology from the University of Calabria. In 2012, she received her Ph.D. (Dr. Rer. Nat.) in Materials for Life Sciences from the University of Potsdam and the Institute of Biomaterials Science (Germany). Subsequently, she worked as postdoctoral research fellow at the University of Surrey (Department of Chemistry, UK) and at the KU Leuven (Department of Materials Engineering and Prometheus Research Division, Belgium). Her research interests include the development of in vitro models for arthritis and of novel hydrogels for applications in drug delivery and regenerative medicine.

David Eglin is Principal Investigator at the AO Research Institute Davos and holds the chair of Translational Biomaterials Research in Orthopedics at the University of Twente, The Netherlands. Following doctoral studies on the topic of composite biomaterials for bone repair at Nottingham Trent University, England, he joined Prof. Jacques Livage group at the laboratory of Chemistry of Condensed Matter at the Collège de France, as a postdoctoral researcher in 2002. In 2006, he joined the AO Research Institute Davos and has since developed biomaterials, such as biopolymers based responsive hydrogels, and additive manufacturing technologies for basic under-

https://dx.doi.org/10.1021/acs.chemrev.0c00084
Chem. Rev. 2020, 120, 11028−11055

standing of biomaterials and cells interaction, and for translational research in the trauma and orthopaedic field.

Jos Malda is full Professor and is chair of Biofabrication in Translational Regenerative Medicine at Utrecht University. He studied Bioprocess Engineering (Wageningen University, 1999) and holds a Ph.D. degree from the University of Twente (2003). In 2004, he became a research fellow at Queensland University of Technology, Australia. He then started in Utrecht in 2007, where his current research focusses on the convergence and application of biofabrication technologies as strategies for the generation of living implants, as well as for advanced in vitro models.

ACKNOWLEDGMENTS

This work is part of the osteochondral defect collaborative research program supported by the AO foundation. The Graubünden Innovationsstiftung, the Dutch Arthritis Society (LLP-12 and LLP-22), and the Gravitation Program "Materials Driven Regeneration", funded by The Netherlands Organization for Scientific Research (024.003.013), are acknowledged for their financial support.

ABBREVIATIONS

3D = three-dimensional
AM = additive manufacturing
CAD = computer-aided design
CT = computed tomography
DLP = digital light projection
DMD = digital micromirror device
ECM = extracellular matrix
FDM = fused deposition modeling
FRESH = freeform reversible embedding of suspended hydrogels
HRP = horseradish peroxidase
H_2O_2 = hydrogen peroxide
MPP = multiphoton polymerization
OCT = optical coherence tomography
PCL = poly(ε-caprolactone)
PLA = polylactic acid
PEG = polyethylene glycol
SLA = stereolithography
VBP = volumetric bioprinting

REFERENCES

(1) Chen, Y.; Li, T.; Jia, Z.; Scarpa, F.; Yao, C.-W.; Wang, L. 3d Printed Hierarchical Honeycombs with Shape Integrity under Large Compressive Deformations. *Mater. Des.* **2018**, *137*, 226−234.
(2) Duan, S.; Tao, Y.; Lei, H.; Wen, W.; Liang, J.; Fang, D. Enhanced out-of-Plane Compressive Strength and Energy Absorption of 3d Printed Square and Hexagonal Honeycombs with Variable-Thickness Cell Edges. *Extreme Mechanics Letters* **2018**, *18*, 9−18.
(3) Nguyen, D. G.; Funk, J.; Robbins, J. B.; Crogan-Grundy, C.; Presnell, S. C.; Singer, T.; Roth, A. B.; Su, B.-L. Bioprinted 3d Primary Liver Tissues Allow Assessment of Organ-Level Response to Clinical Drug Induced Toxicity in Vitro. *PLoS One* **2016**, *11*, e0158674.
(4) Lee, A.; Hudson, A. R.; Shiwarski, D. J.; Tashman, J. W.; Hinton, T. J.; Yerneni, S.; Bliley, J. M.; Campbell, P. G.; Feinberg, A. W. 3d Bioprinting of Collagen to Rebuild Components of the Human Heart. *Science* **2019**, *365*, 482−487.
(5) Moroni, L.; Boland, T.; Burdick, J. A.; De Maria, C.; Derby, B.; Forgacs, G.; Groll, J.; Li, Q.; Malda, J.; Mironov, V. A.; et al. Biofabrication: A Guide to Technology and Terminology. *Trends Biotechnol.* **2018**, *36*, 384−402.
(6) Kang, D.; Hong, G.; An, S.; Jang, I.; Yun, W. S.; Shim, J. H.; Jin, S. Bioprinting of Multiscaled Hepatic Lobules within a Highly Vascularized Construct. *Small* **2020**, *16*, 1905505.
(7) Motealleh, A.; Celebi-Saltik, B.; Ermis, N.; Nowak, S.; Khademhosseini, A.; Kehr, N. S. 3d Printing of Step-Gradient Nanocomposite Hydrogels for Controlled Cell Migration. *Biofabrication* **2019**, *11*, 045015.
(8) Moxon, S. R.; Cooke, M. E.; Cox, S. C.; Snow, M.; Jeys, L.; Jones, S. W.; Smith, A. M.; Grover, L. M. Suspended Manufacture of Biological Structures. *Adv. Mater.* **2017**, *29*, 1605594.
(9) Groll, J.; Boland, T.; Blunk, T.; Burdick, J. A.; Cho, D. W.; Dalton, P. D.; Derby, B.; Forgacs, G.; Li, Q.; Mironov, V. A.; et al. Biofabrication: Reappraising the Definition of an Evolving Field. *Biofabrication* **2016**, *8*, 013001.
(10) Ovsianikov, A.; Muhleder, S.; Torgersen, J.; Li, Z.; Qin, X. H.; Van Vlierberghe, S.; Dubruel, P.; Holnthoner, W.; Redl, H.; Liska, R.; et al. Laser Photofabrication of Cell-Containing Hydrogel Constructs. *Langmuir* **2014**, *30*, 3787−3794.
(11) Bernal, P. N.; Delrot, P.; Loterie, D.; Li, Y.; Malda, J.; Moser, C.; Levato, R. Volumetric Bioprinting of Complex Living-Tissue Constructs within Seconds. *Adv. Mater.* **2019**, *31*, 1904209.
(12) Grigoryan, B.; Paulsen, S. J.; Corbett, D. C.; Sazer, D. W.; Fortin, C. L.; Zaita, A. J.; Greenfield, P. T.; Calafat, N. J.; Gounley, J. P.; Ta, A. H.; et al. Multivascular Networks and Functional Intravascular Topologies within Biocompatible Hydrogels. *Science* **2019**, *364*, 458−464.
(13) Hinton, T. J.; Jallerat, Q.; Palchesko, R. N.; Park, J. H.; Grodzicki, M. S.; Shue, H. J.; Ramadan, M. H.; Hudson, A. R.; Feinberg, A. W. Three-Dimensional Printing of Complex Biological Structures by Freeform Reversible Embedding of Suspended Hydrogels. *Sci. Adv.* **2015**, *1*, e1500758.
(14) Miri, A. K.; Khalilpour, A.; Cecen, B.; Maharjan, S.; Shin, S. R.; Khademhosseini, A. Multiscale Bioprinting of Vascularized Models. *Biomaterials* **2019**, *198*, 204−216.
(15) Gong, J.; Schuurmans, C. C. L.; Genderen, A. M. V.; Cao, X.; Li, W.; Cheng, F.; He, J. J.; Lopez, A.; Huerta, V.; Manriquez, J.; et al. Complexation-Induced Resolution Enhancement of 3d-Printed Hydrogel Constructs. *Nat. Commun.* **2020**, *11*, 1267.
(16) Kesti, M.; Muller, M.; Becher, J.; Schnabelrauch, M.; D'Este, M.; Eglin, D.; Zenobi-Wong, M. A Versatile Bioink for Three-Dimensional Printing of Cellular Scaffolds Based on Thermally and Photo-Triggered Tandem Gelation. *Acta Biomater.* **2015**, *11*, 162−172.
(17) Naghieh, S.; Sarker, M. D.; Sharma, N. K.; Barhoumi, Z.; Chen, X. Printability of 3d Printed Hydrogel Scaffolds: Influence of Hydrogel Composition and Printing Parameters. *Appl. Sci.* **2020**, *10*, 292.
(18) Kang, D.; Ahn, G.; Kim, D.; Kang, H. W.; Yun, S.; Yun, W. S.; Shim, J. H.; Jin, S. Pre-Set Extrusion Bioprinting for Multiscale Heterogeneous Tissue Structure Fabrication. *Biofabrication* **2018**, *10*, 035008.
(19) Miller, J. S.; Burdick, J. A. Editorial: Special Issue on 3d Printing of Biomaterials. *ACS Biomater. Sci. Eng.* **2016**, *2*, 1658−1661.
(20) Groll, J.; Burdick, J. A.; Cho, D. W.; Derby, B.; Gelinsky, M.; Heilshorn, S. C.; Jungst, T.; Malda, J.; Mironov, V. A.; Nakayama, K.; et al. A Definition of Bioinks and Their Distinction from Biomaterial Inks. *Biofabrication* **2019**, *11*, 013001.
(21) Malda, J.; Visser, J.; Melchels, F. P.; Jungst, T.; Hennink, W. E.; Dhert, W. J.; Groll, J.; Hutmacher, D. W. 25th Anniversary Article: Engineering Hydrogels for Biofabrication. *Adv. Mater.* **2013**, *25*, 5011−5028.
(22) Datta, P.; Vyas, V.; Dhara, S.; Chowdhury, A. R.; Barui, A. Anisotropy Properties of Tissues: A Basis for Fabrication of Biomimetic Anisotropic Scaffolds for Tissue Engineering. *Journal of Bionic Engineering* **2019**, *16*, 842−868.
(23) Valot, L.; Martinez, J.; Mehdi, A.; Subra, G. Chemical Insights into Bioinks for 3d Printing. *Chem. Soc. Rev.* **2019**, *48*, 4049−4086.
(24) Derakhshanfar, S.; Mbeleck, R.; Xu, K.; Zhang, X.; Zhong, W.; Xing, M. 3d Bioprinting for Biomedical Devices and Tissue

https://dx.doi.org/10.1021/acs.chemrev.0c00084
Chem. Rev. 2020, 120, 11028−11055

Engineering: A Review of Recent Trends and Advances. *Bioact Mater.* **2018**, *3*, 144−156.
(25) Wlodarczyk-Biegun, M. K.; Del Campo, A. 3d Bioprinting of Structural Proteins. *Biomaterials* **2017**, *134*, 180−201.
(26) Sun, W.; Starly, B.; Daly, A. C.; Burdick, J. A.; Groll, J.; Skeldon, G.; Shu, W.; Sakai, Y.; Shinohara, M.; Nishikawa, M.; et al. The Bioprinting Roadmap. *Biofabrication* **2020**, *12*, 022002.
(27) de Ruijter, M.; Hrynevich, A.; Haigh, J. N.; Hochleitner, G.; Castilho, M.; Groll, J.; Malda, J.; Dalton, P. D. Out-of-Plane 3d-Printed Microfibers Improve the Shear Properties of Hydrogel Composites. *Small* **2018**, *14*, 1702773.
(28) Jiang, T.; Munguia-Lopez, J. G.; Flores-Torres, S.; Kort-Mascort, J.; Kinsella, J. M. Extrusion Bioprinting of Soft Materials: An Emerging Technique for Biological Model Fabrication. *Appl. Phys. Rev.* **2019**, *6*, 011310.
(29) Murphy, S. V.; Atala, A. 3d Bioprinting of Tissues and Organs. *Nat. Biotechnol.* **2014**, *32*, 773−785.
(30) Castilho, M.; de Ruijter, M.; Beirne, S.; Villette, C. C.; Ito, K.; Wallace, G. G.; Malda, J. Multitechnology Biofabrication: A New Approach for the Manufacturing of Functional Tissue Structures? *Trends Biotechnol.* **2020**. DOI: 10.1016/j.tibtech.2020.04.014
(31) Han, J.; Kim, D. S.; Jang, H.; Kim, H. R.; Kang, H. W. Bioprinting of Three-Dimensional Dentin-Pulp Complex with Local Differentiation of Human Dental Pulp Stem Cells. *J. Tissue Eng.* **2019**, *10*, 2041731419845849.
(32) Chen, M.; Feng, Z.; Guo, W.; Yang, D.; Gao, S.; Li, Y.; Shen, S.; Yuan, Z.; Huang, B.; Zhang, Y.; et al. Pcl-Mecm-Based Hydrogel Hybrid Scaffolds and Meniscal Fibrochondrocytes Promote Whole Meniscus Regeneration in a Rabbit Meniscectomy Model. *ACS Appl. Mater. Interfaces* **2019**, *11*, 41626−41639.
(33) Nowicki, M.; Zhu, W.; Sarkar, K.; Rao, R.; Zhang, L. G. 3d Printing Multiphasic Osteochondral Tissue Constructs with Nano to Micro Features Via Pcl Based Bioink. *Bioprinting* **2020**, *17*, e00066.
(34) Bahcecioglu, G.; Hasirci, N.; Bilgen, B.; Hasirci, V. A 3d Printed Pcl/Hydrogel Construct with Zone-Specific Biochemical Composition Mimicking That of the Meniscus. *Biofabrication* **2019**, *11*, 025002.
(35) Visser, J.; Melchels, F. P.; Jeon, J. E.; van Bussel, E. M.; Kimpton, L. S.; Byrne, H. M.; Dhert, W. J.; Dalton, P. D.; Hutmacher, D. W.; Malda, J. Reinforcement of Hydrogels Using Three-Dimensionally Printed Microfibres. *Nat. Commun.* **2015**, *6*, 6933.
(36) Schipani, R.; Scheurer, S.; Florentin, R.; Critchley, S. E.; Kelly, D. J. Reinforcing Interpenetrating Network Hydrogels with 3d Printed Polymer Networks to Engineer Cartilage Mimetic Composites. *Biofabrication* **2020**, *12*, 035011.
(37) Chimene, D.; Kaunas, R.; Gaharwar, A. K. Hydrogel Bioink Reinforcement for Additive Manufacturing: A Focused Review of Emerging Strategies. *Adv. Mater.* **2020**, *32*, 1902026.
(38) Kyle, S.; Jessop, Z. M.; Al-Sabah, A.; Whitaker, I. S. 'Printability' of Candidate Biomaterials for Extrusion Based 3d Printing: State-of-the-Art. *Adv. Healthcare Mater.* **2017**, *6*, 1700264.
(39) Daly, A. C.; Freeman, F. E.; Gonzalez-Fernandez, T.; Critchley, S. E.; Nulty, J.; Kelly, D. J. 3d Bioprinting for Cartilage and Osteochondral Tissue Engineering. *Adv. Healthcare Mater.* **2017**, *6*, 1700298.
(40) Bittner, S. M.; Smith, B. T.; Diaz-Gomez, L.; Hudgins, C. D.; Melchiorri, A. J.; Scott, D. W.; Fisher, J. P.; Mikos, A. G. Fabrication and Mechanical Characterization of 3d Printed Vertical Uniform and Gradient Scaffolds for Bone and Osteochondral Tissue Engineering. *Acta Biomater.* **2019**, *90*, 37−48.
(41) Muller, M.; Ozturk, E.; Arlov, O.; Gatenholm, P.; Zenobi-Wong, M. Alginate Sulfate-Nanocellulose Bioinks for Cartilage Bioprinting Applications. *Ann. Biomed. Eng.* **2017**, *45*, 210−223.
(42) Habib, A.; Sathish, V.; Mallik, S.; Khoda, B. 3d Printability of Alginate-Carboxymethyl Cellulose Hydrogel. *Materials* **2018**, *11*, 454.
(43) Emmermacher, J.; Spura, D.; Cziommer, J.; Kilian, D.; Wollborn, T.; Fritsching, U.; Steingroewer, J.; Walther, T.; Gelinsky, M.; Lode, A. Engineering Considerations on Extrusion-Based Bioprinting: Interactions of Material Behavior, Mechanical Forces and Cells in the Printing Needle. *Biofabrication* **2020**, *12*, 025022.
(44) Ning, L.; Guillemot, A.; Zhao, J.; Kipouros, G.; Chen, X. Influence of Flow Behavior of Alginate-Cell Suspensions on Cell Viability and Proliferation. *Tissue Eng., Part C* **2016**, *22*, 652−662.
(45) Ning, L.; Yang, B.; Mohabatpour, F.; Betancourt, N.; Sarker, M. D.; Papagerakis, P.; Chen, X. Process-Induced Cell Damage: Pneumatic Versus Screw-Driven Bioprinting. *Biofabrication* **2020**, *12*, 025011.
(46) Ouyang, L.; Yao, R.; Zhao, Y.; Sun, W. Effect of Bioink Properties on Printability and Cell Viability for 3d Bioplotting of Embryonic Stem Cells. *Biofabrication* **2016**, *8*, 035020.
(47) Sakai, S.; Kamei, H.; Mori, T.; Hotta, T.; Ohi, H.; Nakahata, M.; Taya, M. Visible Light-Induced Hydrogelation of an Alginate Derivative and Application to Stereolithographic Bioprinting Using a Visible Light Projector and Acid Red. *Biomacromolecules* **2018**, *19*, 672−679.
(48) Olate-Moya, F.; Arens, L.; Wilhelm, M.; Mateos-Timoneda, M. A.; Engel, E.; Palza, H. Chondroinductive Alginate-Based Hydrogels Having Graphene Oxide for 3d Printed Scaffold Fabrication. *ACS Appl. Mater. Interfaces* **2020**, *12*, 4343−4357.
(49) Jiang, T.; Munguia-Lopez, J. G.; Gu, K.; Bavoux, M. M.; Flores-Torres, S.; Kort-Mascort, J.; Grant, J.; Vijayakumar, S.; De Leon-Rodriguez, A.; Ehrlicher, A. J.; et al. Engineering Bioprintable Alginate/Gelatin Composite Hydrogels with Tunable Mechanical and Cell Adhesive Properties to Modulate Tumor Spheroid Growth Kinetics. *Biofabrication* **2020**, *12*, 015024.
(50) Roehm, K. D.; Madihally, S. V. Bioprinted Chitosan-Gelatin Thermosensitive Hydrogels Using an Inexpensive 3d Printer. *Biofabrication* **2018**, *10*, 015002.
(51) Daly, A. C.; Critchley, S. E.; Rencsok, E. M.; Kelly, D. J. A Comparison of Different Bioinks for 3d Bioprinting of Fibrocartilage and Hyaline Cartilage. *Biofabrication* **2016**, *8*, 045002.
(52) López-Marcial, G. R.; Zeng, A. Y.; Osuna, C.; Dennis, J.; García, J. M.; O'Connell, G. D. Agarose-Based Hydrogels as Suitable Bioprinting Materials for Tissue Engineering. *ACS Biomater. Sci. Eng.* **2018**, *4*, 3610−3616.
(53) Gu, Q.; Tomaskovic-Crook, E.; Wallace, G. G.; Crook, J. M. 3d Bioprinting Human Induced Pluripotent Stem Cell Constructs for in Situ Cell Proliferation and Successive Multilineage Differentiation. *Adv. Healthcare Mater.* **2017**, *6*, 1700175.
(54) Diamantides, N.; Dugopolski, C.; Blahut, E.; Kennedy, S.; Bonassar, L. J. High Density Cell Seeding Affects the Rheology and Printability of Collagen Bioinks. *Biofabrication* **2019**, *11*, 045016.
(55) Osidak, E. O.; Karalkin, P. A.; Osidak, M. S.; Parfenov, V. A.; Sivogrivov, D. E.; Pereira, F.; Gryadunova, A. A.; Koudan, E. V.; Khesuani, Y. D.; Capital Ka, C. V. A.; et al. Viscoll Collagen Solution as a Novel Bioink for Direct 3d Bioprinting. *J. Mater. Sci.: Mater. Med.* **2019**, *30*, 31.
(56) Zhang, S.; Huang, D.; Lin, H.; Xiao, Y.; Zhang, X. Cellulose Nanocrystal Reinforced Collagen-Based Nanocomposite Hydrogel with Self-Healing and Stress-Relaxation Properties for Cell Delivery. *Biomacromolecules* **2020**, *21*, 2400−2408.
(57) Choi, D. J.; Kho, Y.; Park, S. J.; Kim, Y. J.; Chung, S.; Kim, C. H. Effect of Cross-Linking on the Dimensional Stability and Biocompatibility of a Tailored 3d-Bioprinted Gelatin Scaffold. *Int. J. Biol. Macromol.* **2019**, *135*, 659−667.
(58) Contessi Negrini, N.; Celikkin, N.; Tarsini, P.; Fare, S.; Swieszkowski, W. Three-Dimensional Printing of Chemically Cross-linked Gelatin Hydrogels for Adipose Tissue Engineering. *Biofabrication* **2020**, *12*, 025001.
(59) Leucht, A.; Volz, A. C.; Rogal, J.; Borchers, K.; Kluger, P. J. Advanced Gelatin-Based Vascularization Bioinks for Extrusion-Based Bioprinting of Vascularized Bone Equivalents. *Sci. Rep.* **2020**, *10*, 5330.
(60) Schwartz, R.; Malpica, M.; Thompson, G. L.; Miri, A. K. Cell Encapsulation in Gelatin Bioink Impairs 3d Bioprinting Resolution. *J. Mech Behav Biomed Mater.* **2020**, *103*, 103524.

(61) Serna, J. A.; Florez, S. L.; Talero, V. A.; Briceno, J. C.; Munoz-Camargo, C.; Cruz, J. C. Formulation and Characterization of a Sis-Based Photocrosslinkable Bioink. *Polymers (Basel, Switz.)* **2019**, *11*, 569.
(62) Kim, M. K.; Jeong, W.; Lee, S. M.; Kim, J. B.; Jin, S.; Kang, H. W. Decellularized Extracellular Matrix-Based Bio-Ink with Enhanced 3d Printability and Mechanical Properties. *Biofabrication* **2020**, *12*, 025003.
(63) Dzobo, K.; Motaung, K. S. C. M.; Adesida, A. Recent Trends in Decellularized Extracellular Matrix Bioinks for 3d Printing: An Updated Review. *Int. J. Mol. Sci.* **2019**, *20*, 4628.
(64) Noh, I.; Kim, N.; Tran, H. N.; Lee, J.; Lee, C. 3d Printable Hyaluronic Acid-Based Hydrogel for Its Potential Application as a Bioink in Tissue Engineering. *Biomater Res.* **2019**, *23*, 3.
(65) Antich, C.; de Vicente, J.; Jimenez, G.; Chocarro, C.; Carrillo, E.; Montanez, E.; Galvez-Martin, P.; Marchal, J. A. Bio-Inspired Hydrogel Composed of Hyaluronic Acid and Alginate as a Potential Bioink for 3d Bioprinting of Articular Cartilage Engineering Constructs. *Acta Biomater.* **2020**, *106*, 114−123.
(66) Lee, J.; Lee, S. H.; Kim, B. S.; Cho, Y. S.; Park, Y. Development and Evaluation of Hyaluronic Acid-Based Hybrid Bio-Ink for Tissue Regeneration. *Tissue Eng. Regener. Med.* **2018**, *15*, 761−769.
(67) Petta, D.; D'Amora, U.; Ambrosio, L.; Grijpma, D. W.; Eglin, D.; D'Este, M. Hyaluronic Acid as a Bioink for Extrusion-Based 3d Printing. *Biofabrication* **2020**, *12*, 032001.
(68) Zheng, Z.; Wu, J.; Liu, M.; Wang, H.; Li, C.; Rodriguez, M. J.; Li, G.; Wang, X.; Kaplan, D. L. 3d Bioprinting of Self-Standing Silk-Based Bioink. *Adv. Healthcare Mater.* **2018**, *7*, 1701026.
(69) Sanz-Fraile, H.; Amoros, S.; Mendizabal, I.; Galvez-Monton, C.; Prat-Vidal, C.; Bayes-Genis, A.; Navajas, D.; Farre, R.; Otero, J. Silk-Reinforced Collagen Hydrogels with Raised Multiscale Stiffness for Mesenchymal Cells 3d Culture. *Tissue Eng., Part A* **2020**, *26*, 358−370.
(70) Bandyopadhyay, A.; Mandal, B. B. A Three-Dimensional Printed Silk-Based Biomimetic Tri-Layered Meniscus for Potential Patient-Specific Implantation. *Biofabrication* **2020**, *12*, 015003.
(71) Boraschi-Diaz, I.; Wang, J.; Mort, J. S.; Komarova, S. V. Collagen Type I as a Ligand for Receptor-Mediated Signaling. *Front. Phys.* **2017**, *5*, 12.
(72) Zeltz, C.; Gullberg, D. The Integrin-Collagen Connection–a Glue for Tissue Repair? *J. Cell Sci.* **2016**, *129*, 653−664.
(73) Davidenko, N.; Schuster, C. F.; Bax, D. V.; Farndale, R. W.; Hamaia, S.; Best, S. M.; Cameron, R. E. Evaluation of Cell Binding to Collagen and Gelatin: A Study of the Effect of 2d and 3d Architecture and Surface Chemistry. *J. Mater. Sci.: Mater. Med.* **2016**, *27*, 148.
(74) Wang, K.; Nune, K. C.; Misra, R. D. The Functional Response of Alginate-Gelatin-Nanocrystalline Cellulose Injectable Hydrogels toward Delivery of Cells and Bioactive Molecules. *Acta Biomater.* **2016**, *36*, 143−151.
(75) Mosesson, M. W.; Siebenlist, K. R.; Meh, D. A. The Structure and Biological Features of Fibrinogen and Fibrin. *Ann. N. Y. Acad. Sci.* **2001**, *936*, 11−30.
(76) Mosesson, M. W. Fibrinogen and Fibrin Structure and Functions. *J. Thromb. Haemostasis* **2005**, *3*, 1894−1904.
(77) Rutz, A. L.; Hyland, K. E.; Jakus, A. E.; Burghardt, W. R.; Shah, R. N. A Multimaterial Bioink Method for 3d Printing Tunable, Cell-Compatible Hydrogels. *Adv. Mater.* **2015**, *27*, 1607−1614.
(78) Ribeiro, A.; Blokzijl, M. M.; Levato, R.; Visser, C. W.; Castilho, M.; Hennink, W. E.; Vermonden, T.; Malda, J. Assessing Bioink Shape Fidelity to Aid Material Development in 3d Bioprinting. *Biofabrication* **2018**, *10*, 014102.
(79) Hospodiuk, M.; Dey, M.; Sosnoski, D.; Ozbolat, I. T. The Bioink: A Comprehensive Review on Bioprintable Materials. *Biotechnol. Adv.* **2017**, *35*, 217−239.
(80) Leberfinger, A. N.; Ravnic, D. J.; Dhawan, A.; Ozbolat, I. T. Concise Review: Bioprinting of Stem Cells for Transplantable Tissue Fabrication. *Stem Cells Transl. Med.* **2017**, *6*, 1940−1948.
(81) Mahzoon, S.; Siahaan, T. J.; Detamore, M. S. In *Bio-Instructive Scaffolds for Musculoskeletal Tissue Engineering and Regenerative Medicine*; Brown, J. L., Kumbar, S. G., Banik, B. L., Eds.; Academic Press, 2017; DOI: 10.1016/b978-0-12-803394-4.00002-1 .
(82) Wang, C.; Liu, Y.; Fan, Y.; Li, X. The Use of Bioactive Peptides to Modify Materials for Bone Tissue Repair. *Regen Biomater* **2017**, *4*, 191−206.
(83) Bicho, D.; Ajami, S.; Liu, C.; Reis, R. L.; Oliveira, J. M. Peptide-Biofunctionalization of Biomaterials for Osteochondral Tissue Regeneration in Early Stage Osteoarthritis: Challenges and Opportunities. *J. Mater. Chem. B* **2019**, *7*, 1027−1044.
(84) Hosoyama, K.; Lazurko, C.; Munoz, M.; McTiernan, C. D.; Alarcon, E. I. Peptide-Based Functional Biomaterials for Soft-Tissue Repair. *Front. Bioeng. Biotechnol.* **2019**, *7*, 205.
(85) Tallawi, M.; Rosellini, E.; Barbani, N.; Cascone, M. G.; Rai, R.; Saint-Pierre, G.; Boccaccini, A. R. Strategies for the Chemical and Biological Functionalization of Scaffolds for Cardiac Tissue Engineering: A Review. *J. R. Soc., Interface* **2015**, *12*, 20150254.
(86) Patterson, J.; Hubbell, J. A. Enhanced Proteolytic Degradation of Molecularly Engineered Peg Hydrogels in Response to Mmp-1 and Mmp-2. *Biomaterials* **2010**, *31*, 7836−7845.
(87) Jungst, T.; Smolan, W.; Schacht, K.; Scheibel, T.; Groll, J. Strategies and Molecular Design Criteria for 3d Printable Hydrogels. *Chem. Rev.* **2016**, *116*, 1496−1539.
(88) Gungor-Ozkerim, P. S.; Inci, I.; Zhang, Y. S.; Khademhosseini, A.; Dokmeci, M. R. Bioinks for 3d Bioprinting: An Overview. *Biomater. Sci.* **2018**, *6*, 915−946.
(89) Liu, J.; Sun, L.; Xu, W.; Wang, Q.; Yu, S.; Sun, J. Current Advances and Future Perspectives of 3d Printing Natural-Derived Biopolymers. *Carbohydr. Polym.* **2019**, *207*, 297−316.
(90) Li, H.; Tan, C.; Li, L. Review of 3d Printable Hydrogels and Constructs. *Mater. Des.* **2018**, *159*, 20−38.
(91) Foyt, D. A.; Norman, M. D. A.; Yu, T. T. L.; Gentleman, E. Exploiting Advanced Hydrogel Technologies to Address Key Challenges in Regenerative Medicine. *Adv. Healthcare Mater.* **2018**, *7*, 1700939.
(92) Levato, R.; Jungst, T.; Scheuring, R. G.; Blunk, T.; Groll, J.; Malda, J. From Shape to Function: The Next Step in Bioprinting. *Adv. Mater.* **2020**, *32*, 1906423.
(93) Morgan, F. L. C.; Moroni, L.; Baker, M. B. Dynamic Bioinks to Advance Bioprinting. *Adv. Healthcare Mater.* **2020**, *9*, 1901798.
(94) Hölzl, K.; Lin, S.; Tytgat, L.; Van Vlierberghe, S.; Gu, L.; Ovsianikov, A. Bioink Properties before, During and after 3d Bioprinting. *Biofabrication* **2016**, *8*, 032002.
(95) Tabriz, A. G.; Hermida, M. A.; Leslie, N. R.; Shu, W. Three-Dimensional Bioprinting of Complex Cell Laden Alginate Hydrogel Structures. *Biofabrication* **2015**, *7*, 045012.
(96) Kumar, A.; Srivastava, A.; Galaev, I. Y.; Mattiasson, B. Smart Polymers: Physical Forms and Bioengineering Applications. *Prog. Polym. Sci.* **2007**, *32*, 1205−1237.
(97) Cochis, A.; Bonetti, L.; Sorrentino, R.; Contessi Negrini, N.; Grassi, F.; Leigheb, M.; Rimondini, L.; Fare, S. 3d Printing of Thermo-Responsive Methylcellulose Hydrogels for Cell-Sheet Engineering. *Materials* **2018**, *11*, 579.
(98) Gu, Z.; Gao, Z.; Liu, W.; Wen, Y.; Gu, Q. A Facile Method to Fabricate Anisotropic Extracellular Matrix with 3d Printing Topological Microfibers. *Materials* **2019**, *12*, 3944.
(99) Sarker, M. D.; Naghieh, S.; McInnes, A. D.; Ning, L.; Schreyer, D. J.; Chen, X. Bio-Fabrication of Peptide-Modified Alginate Scaffolds: Printability, Mechanical Stability and Neurite Outgrowth Assessments. *Bioprinting* **2019**, *14*, e00045.
(100) Sarker, M.; Chen, X. B. Modeling the Flow Behavior and Flow Rate of Medium Viscosity Alginate for Scaffold Fabrication with a Three-Dimensional Bioplotter. *J. Manuf. Sci. Eng.* **2017**, *139*, 081002.
(101) Suntornnond, R.; Tan, E. Y. S.; An, J.; Chua, C. K. A Highly Printable and Biocompatible Hydrogel Composite for Direct Printing of Soft and Perfusable Vasculature-Like Structures. *Sci. Rep.* **2017**, *7*, 16902.
(102) Muller, M.; Becher, J.; Schnabelrauch, M.; Zenobi-Wong, M. Nanostructured Pluronic Hydrogels as Bioinks for 3d Bioprinting. *Biofabrication* **2015**, *7*, 035006.

(103) Xin, S.; Chimene, D.; Garza, J. E.; Gaharwar, A. K.; Alge, D. L. Clickable Peg Hydrogel Microspheres as Building Blocks for 3d Bioprinting. *Biomater. Sci.* **2019**, *7*, 1179−1187.
(104) Highley, C. B.; Song, K. H.; Daly, A. C.; Burdick, J. A. Jammed Microgel Inks for 3d Printing Applications. *Adv. Sci. (Weinh)* **2019**, *6*, 1801076.
(105) Petta, D.; Grijpma, D. W.; Alini, M.; Eglin, D.; D'Este, M. Three-Dimensional Printing of a Tyramine Hyaluronan Derivative with Double Gelation Mechanism for Independent Tuning of Shear Thinning and Postprinting Curing. *ACS Biomater. Sci. Eng.* **2018**, *4*, 3088−3098.
(106) Rodell, C. B.; Kaminski, A. L.; Burdick, J. A. Rational Design of Network Properties in Guest-Host Assembled and Shear-Thinning Hyaluronic Acid Hydrogels. *Biomacromolecules* **2013**, *14*, 4125−4134.
(107) Rodell, C. B.; MacArthur, J. W., Jr; Dorsey, S. M.; Wade, R. J.; Wang, L. L.; Woo, Y. J.; Burdick, J. A. Shear-Thinning Supramolecular Hydrogels with Secondary Autonomous Covalent Crosslinking to Modulate Viscoelastic Properties in Vivo. *Adv. Funct. Mater.* **2015**, *25*, 636−644.
(108) Lim, K. S.; Galarraga, J. H.; Cui, X.; Lindberg, G. C. J.; Burdick, J. A.; Woodfield, T. B. F. Fundamentals and Applications of Photo-Cross-Linking in Bioprinting. *Chem. Rev.* **2020**. DOI: 10.1021/acs.chemrev.9b00812
(109) Hu, W.; Wang, Z.; Xiao, Y.; Zhang, S.; Wang, J. Advances in Crosslinking Strategies of Biomedical Hydrogels. *Biomater. Sci.* **2019**, *7*, 843−855.
(110) Liu, M.; Zeng, X.; Ma, C.; Yi, H.; Ali, Z.; Mou, X.; Li, S.; Deng, Y.; He, N. Injectable Hydrogels for Cartilage and Bone Tissue Engineering. *Bone Res.* **2017**, *5*, 17014.
(111) Park, K. M.; Park, K. D. In Situ Cross-Linkable Hydrogels as a Dynamic Matrix for Tissue Regenerative Medicine. *Tissue Eng. Regener. Med.* **2018**, *15*, 547−557.
(112) Cui, X.; Li, J.; Hartanto, Y.; Durham, M.; Tang, J.; Zhang, H.; Hooper, G.; Lim, K.; Woodfield, T. Advances in Extrusion 3d Bioprinting: A Focus on Multicomponent Hydrogel-Based Bioinks. *Adv. Healthcare Mater.* **2020**, *9*, 1901648.
(113) Widel, M.; Krzywon, A.; Gajda, K.; Skonieczna, M.; Rzeszowska-Wolny, J. Induction of Bystander Effects by Uva, Uvb, and Uvc Radiation in Human Fibroblasts and the Implication of Reactive Oxygen Species. *Free Radical Biol. Med.* **2014**, *68*, 278−287.
(114) Lee, C.; O'Connell, C. D.; Onofrillo, C.; Choong, P. F. M.; Di Bella, C.; Duchi, S. Human Articular Cartilage Repair: Sources and Detection of Cytotoxicity and Genotoxicity in Photo-Crosslinkable Hydrogel Bioscaffolds. *Stem Cells Transl. Med.* **2020**, *9*, 302−315.
(115) Stichler, S.; Bock, T.; Paxton, N.; Bertlein, S.; Levato, R.; Schill, V.; Smolan, W.; Malda, J.; Tessmar, J.; Blunk, T.; et al. Double Printing of Hyaluronic Acid/Poly(Glycidol) Hybrid Hydrogels with Poly(ε-Caprolactone) for Msc Chondrogenesis. *Biofabrication* **2017**, *9*, 044108.
(116) Duchi, S.; Onofrillo, C.; O'Connell, C. D.; Blanchard, R.; Augustine, C.; Quigley, A. F.; Kapsa, R. M. I.; Pivonka, P.; Wallace, G.; Di Bella, C.; Choong, P. F. M. Handheld Co-Axial Bioprinting: Application to in Situ Surgical Cartilage Repair. *Sci. Rep.* **2017**, *7*, 5837.
(117) Lin, H.; Zhang, D.; Alexander, P. G.; Yang, G.; Tan, J.; Cheng, A. W.; Tuan, R. S. Application of Visible Light-Based Projection Stereolithography for Live Cell-Scaffold Fabrication with Designed Architecture. *Biomaterials* **2013**, *34*, 331−339.
(118) Bahney, C. S.; Lujan, T. J.; Hsu, C. W.; Bottlang, M.; West, J. L.; Johnstone, B. Visible Light Photoinitiation of Mesenchymal Stem Cell-Laden Bioresponsive Hydrogels. *Eur. Cell Mater.* **2011**, *22*, 43−55 discussion 55.
(119) Lim, K. S.; Schon, B. S.; Mekhileri, N. V.; Brown, G. C. J.; Chia, C. M.; Prabakar, S.; Hooper, G. J.; Woodfield, T. B. F. New Visible-Light Photoinitiating System for Improved Print Fidelity in Gelatin-Based Bioinks. *ACS Biomater. Sci. Eng.* **2016**, *2*, 1752−1762.
(120) Mazaki, T.; Shiozaki, Y.; Yamane, K.; Yoshida, A.; Nakamura, M.; Yoshida, Y.; Zhou, D.; Kitajima, T.; Tanaka, M.; Ito, Y.; Ozaki, T.; Matsukawa, A. A Novel, Visible Light-Induced, Rapidly Cross-Linkable Gelatin Scaffold for Osteochondral Tissue Engineering. *Sci. Rep.* **2015**, *4*, 4457.
(121) Fedorovich, N. E.; Swennen, I.; Girones, J.; Moroni, L.; van Blitterswijk, C. A.; Schacht, E.; Alblas, J.; Dhert, W. J. Evaluation of Photocrosslinked Lutrol Hydrogel for Tissue Printing Applications. *Biomacromolecules* **2009**, *10*, 1689−1696.
(122) Moreira Teixeira, L. S.; Feijen, J.; van Blitterswijk, C. A.; Dijkstra, P. J.; Karperien, M. Enzyme-Catalyzed Crosslinkable Hydrogels: Emerging Strategies for Tissue Engineering. *Biomaterials* **2012**, *33*, 1281−1290.
(123) Broguiere, N.; Formica, F. A.; Barreto, G.; Zenobi-Wong, M. Sortase a as a Cross-Linking Enzyme in Tissue Engineering. *Acta Biomater.* **2018**, *77*, 182−190.
(124) Khanmohammadi, M.; Dastjerdi, M. B.; Ai, A.; Ahmadi, A.; Godarzi, A.; Rahimi, A.; Ai, J. Horseradish Peroxidase-Catalyzed Hydrogelation for Biomedical Applications. *Biomater. Sci.* **2018**, *6*, 1286−1298.
(125) Petta, D.; Armiento, A. R.; Grijpma, D.; Alini, M.; Eglin, D.; D'Este, M. 3d Bioprinting of a Hyaluronan Bioink through Enzymatic- and Visible Light-Crosslinking. *Biofabrication* **2018**, *10*, 044104.
(126) Chimene, D.; Kaunas, R.; Gaharwar, A. K. Hydrogel Bioink Reinforcement for Additive Manufacturing: A Focused Review of Emerging Strategies. *Adv. Mater.* **2020**, *32*, 1902026.
(127) Cowie, J.; Arrighi, V. *Polymers: Chemistry and Physics of Modern Materials*, 3rd ed.; CRC Press, 2007.
(128) Cheremisinoff, N. *Introduction to Polymer Rheology and Processing*; CRC Press, 1993.
(129) Mezger, T. G. *The Rheology Handbook*, 3rd revised ed.; Vincentz Network, 2011.
(130) Ji, S.; Guvendiren, M. Recent Advances in Bioink Design for 3d Bioprinting of Tissues and Organs. *Front. Bioeng. Biotechnol.* **2017**, *5*, 23.
(131) Ramirez Caballero, S. S.; Saiz, E.; Montembault, A.; Tadier, S.; Maire, E.; David, L.; Delair, T.; Gremillard, L. 3-D Printing of Chitosan-Calcium Phosphate Inks: Rheology, Interactions and Characterization. *J. Mater. Sci.: Mater. Med.* **2019**, *30*, 6.
(132) Montufar, E. B.; Maazouz, Y.; Ginebra, M. P. Relevance of the Setting Reaction to the Injectability of Tricalcium Phosphate Pastes. *Acta Biomater.* **2013**, *9*, 6188−6198.
(133) Xu, H. H.; Wang, P.; Wang, L.; Bao, C.; Chen, Q.; Weir, M. D.; Chow, L. C.; Zhao, L.; Zhou, X.; Reynolds, M. A. Calcium Phosphate Cements for Bone Engineering and Their Biological Properties. *Bone Res.* **2017**, *5*, 17056.
(134) Wilson, S. A.; Cross, L. M.; Peak, C. W.; Gaharwar, A. K. Shear-Thinning and Thermo-Reversible Nanoengineered Inks for 3d Bioprinting. *ACS Appl. Mater. Interfaces* **2017**, *9*, 43449−43458.
(135) Chimene, D.; Peak, C. W.; Gentry, J. L.; Carrow, J. K.; Cross, L. M.; Mondragon, E.; Cardoso, G. B.; Kaunas, R.; Gaharwar, A. K. Nanoengineered Ionic-Covalent Entanglement (Nice) Bioinks for 3d Bioprinting. *ACS Appl. Mater. Interfaces* **2018**, *10*, 9957−9968.
(136) Lokhande, G.; Carrow, J. K.; Thakur, T.; Xavier, J. R.; Parani, M.; Bayless, K. J.; Gaharwar, A. K. Nanoengineered Injectable Hydrogels for Wound Healing Application. *Acta Biomater.* **2018**, *70*, 35−47.
(137) Peak, C. W.; Stein, J.; Gold, K. A.; Gaharwar, A. K. Nanoengineered Colloidal Inks for 3d Bioprinting. *Langmuir* **2018**, *34*, 917−925.
(138) Heinemann, S.; Rossler, S.; Lemm, M.; Ruhnow, M.; Nies, B. Properties of Injectable Ready-to-Use Calcium Phosphate Cement Based on Water-Immiscible Liquid. *Acta Biomater.* **2013**, *9*, 6199−6207.
(139) Akkineni, A. R.; Ahlfeld, T.; Lode, A.; Gelinsky, M. A Versatile Method for Combining Different Biopolymers in a Core/Shell Fashion by 3d Plotting to Achieve Mechanically Robust Constructs. *Biofabrication* **2016**, *8*, 045001.
(140) Ouyang, L.; Highley, C. B.; Rodell, C. B.; Sun, W.; Burdick, J. A. 3d Printing of Shear-Thinning Hyaluronic Acid Hydrogels with Secondary Cross-Linking. *ACS Biomater. Sci. Eng.* **2016**, *2*, 1743−1751.

(141) Mouser, V. H.; Melchels, F. P.; Visser, J.; Dhert, W. J.; Gawlitta, D.; Malda, J. Yield Stress Determines Bioprintability of Hydrogels Based on Gelatin-Methacryloyl and Gellan Gum for Cartilage Bioprinting. *Biofabrication* **2016**, *8*, 035003.
(142) Kim, M. H.; Lee, Y. W.; Jung, W. K.; Oh, J.; Nam, S. Y. Enhanced Rheological Behaviors of Alginate Hydrogels with Carrageenan for Extrusion-Based Bioprinting. *J. Mech Behav Biomed Mater.* **2019**, *98*, 187−194.
(143) Highley, C. B.; Rodell, C. B.; Burdick, J. A. Direct 3d Printing of Shear-Thinning Hydrogels into Self-Healing Hydrogels. *Adv. Mater.* **2015**, *27*, 5075−5079.
(144) Paxton, N.; Smolan, W.; Bock, T.; Melchels, F.; Groll, J.; Jungst, T. Proposal to Assess Printability of Bioinks for Extrusion-Based Bioprinting and Evaluation of Rheological Properties Governing Bioprintability. *Biofabrication* **2017**, *9*, 044107.
(145) Skardal, A.; Zhang, J.; Prestwich, G. D. Bioprinting Vessel-Like Constructs Using Hyaluronan Hydrogels Crosslinked with Tetrahedral Polyethylene Glycol Tetracrylates. *Biomaterials* **2010**, *31*, 6173−6181.
(146) Billiet, T.; Gevaert, E.; De Schryver, T.; Cornelissen, M.; Dubruel, P. The 3d Printing of Gelatin Methacrylamide Cell-Laden Tissue-Engineered Constructs with High Cell Viability. *Biomaterials* **2014**, *35*, 49−62.
(147) Skylar-Scott, M. A.; Uzel, S. G. M.; Nam, L. L.; Ahrens, J. H.; Truby, R. L.; Damaraju, S.; Lewis, J. A. Biomanufacturing of Organ-Specific Tissues with High Cellular Density and Embedded Vascular Channels. *Sci. Adv.* **2019**, *5*, eaaw2459.
(148) Jeon, O.; Lee, Y. B.; Jeong, H.; Lee, S. J.; Wells, D.; Alsberg, E. Individual Cell-Only Bioink and Photocurable Supporting Medium for 3d Printing and Generation of Engineered Tissues with Complex Geometries. *Mater. Horiz.* **2019**, *6*, 1625−1631.
(149) Guilak, F.; Jones, W. R.; Ting-Beall, H. P.; Lee, G. M. The Deformation Behavior and Mechanical Properties of Chondrocytes in Articular Cartilage. *Osteoarthritis Cartilage* **1999**, *7*, 59−70.
(150) Guilak, F.; Alexopoulos, L. G.; Haider, M. A.; Ting-Beall, H. P.; Setton, L. A. Zonal Uniformity in Mechanical Properties of the Chondrocyte Pericellular Matrix: Micropipette Aspiration of Canine Chondrons Isolated by Cartilage Homogenization. *Ann. Biomed. Eng.* **2005**, *33*, 1312−1318.
(151) Kiyotake, E. A.; Douglas, A. W.; Thomas, E. E.; Nimmo, S. L.; Detamore, M. S. Development and Quantitative Characterization of the Precursor Rheology of Hyaluronic Acid Hydrogels for Bioprinting. *Acta Biomater.* **2019**, *95*, 176−187.
(152) Behrendt, P.; Ladner, Y.; Stoddart, M. J.; Lippross, S.; Alini, M.; Eglin, D.; Armiento, A. R. Articular Joint-Simulating Mechanical Load Activates Endogenous Tgf-Beta in a Highly Cellularized Bioadhesive Hydrogel for Cartilage Repair. *Am. J. Sports Med.* **2020**, *48*, 210−221.
(153) Cengiz, N.; Gevrek, T. N.; Sanyal, R.; Sanyal, A. Orthogonal Thiol-Ene 'Click' Reactions: A Powerful Combination for Fabrication and Functionalization of Patterned Hydrogels. *Chem. Commun. (Cambridge, U. K.)* **2017**, *53*, 8894−8897.
(154) Wang, L. L.; Highley, C. B.; Yeh, Y. C.; Galarraga, J. H.; Uman, S.; Burdick, J. A. Three-Dimensional Extrusion Bioprinting of Single- and Double-Network Hydrogels Containing Dynamic Covalent Crosslinks. *J. Biomed. Mater. Res., Part A* **2018**, *106*, 865−875.
(155) Sakai, S.; Mochizuki, K.; Qu, Y.; Mail, M.; Nakahata, M.; Taya, M. Peroxidase-Catalyzed Microextrusion Bioprinting of Cell-Laden Hydrogel Constructs in Vaporized Ppm-Level Hydrogen Peroxide. *Biofabrication* **2018**, *10*, 045007.
(156) Petta, D.; Grijpma, D. W.; Alini, M.; Eglin, D.; D'Este, M. Three-Dimensional Printing of a Tyramine Hyaluronan Derivative with Double Gelation Mechanism for Independent Tuning of Shear Thinning and Postprinting Curing. *ACS Biomater. Sci. Eng.* **2018**, *4*, 3088−3098.
(157) Irvine, S.; Agrawal, A.; Lee, B. H.; Chua, H. Y.; Low, K. Y.; Lau, B. C.; Machluff, M.; Venkatraman, S. 3d Printing Structures with a Cell Bearing Gelatin Bioink and Transglutaminase Crosslinking. *Front. Bioeng. Biotechnol.* **2016**.4 DOI: 10.3389/conf.FBIOE.2016.01.01924
(158) Zhou, M.; Lee, B. H.; Tan, Y. J.; Tan, L. P. Microbial Transglutaminase Induced Controlled Crosslinking of Gelatin Methacryloyl to Tailor Rheological Properties for 3d Printing. *Biofabrication* **2019**, *11*, 025011.
(159) Pimentel C, R.; Ko, S. K.; Caviglia, C.; Wolff, A.; Emneus, J.; Keller, S. S.; Dufva, M. Three-Dimensional Fabrication of Thick and Densely Populated Soft Constructs with Complex and Actively Perfused Channel Network. *Acta Biomater.* **2018**, *65*, 174−184.
(160) Gillispie, G.; Prim, P.; Copus, J.; Fisher, J.; Mikos, A. G.; Yoo, J. J.; Atala, A.; Lee, S. J. Assessment Methodologies for Extrusion-Based Bioink Printability. *Biofabrication* **2020**, *12*, 022003.
(161) Kiyotake, E. A.; Douglas, A. W.; Thomas, E. E.; Nimmo, S. L.; Detamore, M. S. Development and Quantitative Characterization of the Precursor Rheology of Hyaluronic Acid Hydrogels for Bioprinting. *Acta Biomater.* **2019**, *95*, 176.
(162) Gao, T.; Gillispie, G. J.; Copus, J. S.; Pr, A. K.; Seol, Y. J.; Atala, A.; Yoo, J. J.; Lee, S. J. Optimization of Gelatin-Alginate Composite Bioink Printability Using Rheological Parameters: A Systematic Approach. *Biofabrication* **2018**, *10*, 034106.
(163) Soltan, N.; Ning, L.; Mohabatpour, F.; Papagerakis, P.; Chen, X. Printability and Cell Viability in Bioprinting Alginate Dialdehyde-Gelatin Scaffolds. *ACS Biomater. Sci. Eng.* **2019**, *5*, 2976−2987.
(164) Wypych, G. *Typical Methods of Quality Control of Plasticizers.* **2017**, 85−109.
(165) Peak, C. W.; Singh, K. A.; Adlouni, M.; Chen, J.; Gaharwar, A. K. Printing Therapeutic Proteins in 3d Using Nanoengineered Bioink to Control and Direct Cell Migration. *Adv. Healthcare Mater.* **2019**, *8*, 1801553.
(166) Pakutsah, K.; Aht-Ong, D. Facile Isolation of Cellulose Nanofibers from Water Hyacinth Using Water-Based Mechanical Defibrillation: Insights into Morphological, Physical, and Rheological Properties. *Int. J. Biol. Macromol.* **2020**, *145*, 64−76.
(167) Ng, W. L.; Lee, J. M.; Zhou, M.; Chen, Y.-W.; Lee, K.-X. A.; Yeong, W. Y.; Shen, Y.-F. Vat Polymerization-Based Bioprinting − Process, Materials, Applications and Regulatory Challenges. *Biofabrication* **2020**, *12*, 022001.
(168) Muller, M.; Fisch, P.; Molnar, M.; Eggert, S.; Binelli, M.; Maniura-Weber, K.; Zenobi-Wong, M. Development and Thorough Characterization of the Processing Steps of an Ink for 3d Printing for Bone Tissue Engineering. *Mater. Sci. Eng., C* **2020**, *108*, 110510.
(169) Schuurman, W.; Levett, P. A.; Pot, M. W.; van Weeren, P. R.; Dhert, W. J.; Hutmacher, D. W.; Melchels, F. P.; Klein, T. J.; Malda, J. Gelatin-Methacrylamide Hydrogels as Potential Biomaterials for Fabrication of Tissue-Engineered Cartilage Constructs. *Macromol. Biosci.* **2013**, *13*, 551−561.
(170) O'Connell, C.; Ren, J.; Pope, L.; Li, Y.; Mohandas, A.; Blanchard, R.; Duchi, S.; Onofrillo, C. Characterizing Bioinks for Extrusion Bioprinting: Printability and Rheology. *Methods Mol. Biol.* **2020**, *2140*, 111−133.
(171) Meng, Y.; Cao, J.; Chen, Y.; Yu, Y.; Ye, L. 3d Printing of a Poly(Vinyl Alcohol)-Based Nano-Composite Hydrogel as an Artificial Cartilage Replacement and the Improvement Mechanism of Printing Accuracy. *J. Mater. Chem. B* **2020**, *8*, 677−690.
(172) Therriault, D.; White, S. R.; Lewis, J. A. Rheological Behavior of Fugitive Organic Inks for Direct-Write Assembly. *Appl. Rheol.* **2007**, *17*, 10112−1.
(173) Lee, Y. B.; Polio, S.; Lee, W.; Dai, G.; Menon, L.; Carroll, R. S.; Yoo, S. S. Bio-Printing of Collagen and Vegf-Releasing Fibrin Gel Scaffolds for Neural Stem Cell Culture. *Exp. Neurol.* **2010**, *223*, 645−652.
(174) Lee, M.; Bae, K.; Levinson, C.; Zenobi-Wong, M. Nanocomposite Bioink Exploits Dynamic Covalent Bonds between Nanoparticles and Polysaccharides for Precision Bioprinting. *Biofabrication* **2020**, *12*, 025025.
(175) Mouser, V. H. M.; Levato, R.; Mensinga, A.; Dhert, W. J. A.; Gawlitta, D.; Malda, J. Bio-Ink Development for Three-Dimensional

https://dx.doi.org/10.1021/acs.chemrev.0c00084
Chem. Rev. 2020, 120, 11028−11055

Bioprinting of Hetero-Cellular Cartilage Constructs. *Connect. Tissue Res.* **2020**, *61*, 137−151.
(176) Wust, S.; Godla, M. E.; Muller, R.; Hofmann, S. Tunable Hydrogel Composite with Two-Step Processing in Combination with Innovative Hardware Upgrade for Cell-Based Three-Dimensional Bioprinting. *Acta Biomater.* **2014**, *10*, 630−640.
(177) Xu, X.; Jagota, A.; Peng, S.; Luo, D.; Wu, M.; Hui, C. Y. Gravity and Surface Tension Effects on the Shape Change of Soft Materials. *Langmuir* **2013**, *29*, 8665−8674.
(178) Wang, L.; Xu, M. E.; Luo, L.; Zhou, Y.; Si, P. Iterative Feedback Bio-Printing-Derived Cell-Laden Hydrogel Scaffolds with Optimal Geometrical Fidelity and Cellular Controllability. *Sci. Rep.* **2018**, *8*, 2802.
(179) Chung, J. H. Y.; Naficy, S.; Yue, Z.; Kapsa, R.; Quigley, A.; Moulton, S. E.; Wallace, G. G. Bio-Ink Properties and Printability for Extrusion Printing Living Cells. *Biomater. Sci.* **2013**, *1*, 763−773.
(180) Shin, J. Y.; Yeo, Y. H.; Jeong, J. E.; Park, S. A.; Park, W. H. Dual-Crosslinked Methylcellulose Hydrogels for 3d Bioprinting Applications. *Carbohydr. Polym.* **2020**, *238*, 116192.
(181) Gohl, J.; Markstedt, K.; Mark, A.; Hakansson, K.; Gatenholm, P.; Edelvik, F. Simulations of 3d Bioprinting: Predicting Bioprintability of Nanofibrillar Inks. *Biofabrication* **2018**, *10*, 034105.
(182) Ahn, G.; Min, K. H.; Kim, C.; Lee, J. S.; Kang, D.; Won, J. Y.; Cho, D. W.; Kim, J. Y.; Jin, S.; Yun, W. S.; Shim, J.-H. Precise Stacking of Decellularized Extracellular Matrix Based 3d Cell-Laden Constructs by a 3d Cell Printing System Equipped with Heating Modules. *Sci. Rep.* **2017**, *7*, 8624.
(183) Athirasala, A.; Tahayeri, A.; Thrivikraman, G.; Franca, C. M.; Monteiro, N.; Tran, V.; Ferracane, J.; Bertassoni, L. E. A Dentin-Derived Hydrogel Bioink for 3d Bioprinting of Cell Laden Scaffolds for Regenerative Dentistry. *Biofabrication* **2018**, *10*, 024101.
(184) Melchels, F. P. W.; Dhert, W. J. A.; Hutmacher, D. W.; Malda, J. Development and Characterisation of a New Bioink for Additive Tissue Manufacturing. *J. Mater. Chem. B* **2014**, *2*, 2282−2289.
(185) Webb, B.; Doyle, B. J. Parameter Optimization for 3d Bioprinting of Hydrogels. *Bioprinting* **2017**, *8*, 8−12.
(186) Di Giuseppe, M.; Law, N.; Webb, B.; Macrae, R. A.; Liew, L. J.; Sercombe, T. B.; Dilley, R. J.; Doyle, B. J. Mechanical Behaviour of Alginate-Gelatin Hydrogels for 3d Bioprinting. *J. Mech Behav. Biomed Mater.* **2018**, *79*, 150−157.
(187) Comeau, P. A.; Willett, T. L. Triethyleneglycol Dimethacrylate Addition Improves the 3d-Printability and Construct Properties of a Gelma-Nha Composite System Towards Tissue Engineering Applications. *Mater. Sci. Eng., C* **2020**, *112*, 110937.
(188) Deo, K. A.; Singh, K. A.; Peak, C. W.; Alge, D. L.; Gaharwar, A. K. Bioprinting 101: Design, Fabrication, and Evaluation of Cell-Laden 3d Bioprinted Scaffolds. *Tissue Eng., Part A* **2020**, *26*, 318−338.
(189) Li, H.; Tan, Y. J.; Liu, S.; Li, L. Three-Dimensional Bioprinting of Oppositely Charged Hydrogels with Super Strong Interface Bonding. *ACS Appl. Mater. Interfaces* **2018**, *10*, 11164−11174.
(190) Diamantides, N.; Wang, L.; Pruiksma, T.; Siemiatkoski, J.; Dugopolski, C.; Shortkroff, S.; Kennedy, S.; Bonassar, L. J. Correlating Rheological Properties and Printability of Collagen Bioinks: The Effects of Riboflavin Photocrosslinking and Ph. *Biofabrication* **2017**, *9*, 034102.
(191) Duarte Campos, D. F.; Blaeser, A.; Korsten, A.; Neuss, S.; Jakel, J.; Vogt, M.; Fischer, H. The Stiffness and Structure of Three-Dimensional Printed Hydrogels Direct the Differentiation of Mesenchymal Stromal Cells toward Adipogenic and Osteogenic Lineages. *Tissue Eng., Part A* **2015**, *21*, 740−756.
(192) Wang, L.; Xu, M.; Zhang, L.; Zhou, Q.; Luo, L. Automated Quantitative Assessment of Three-Dimensional Bioprinted Hydrogel Scaffolds Using Optical Coherence Tomography. *Biomed. Opt. Express* **2016**, *7*, 894−910.
(193) Porter, S. M.; Dailey, H. L.; Hollar, K. A.; Klein, K.; Harty, J. A.; Lujan, T. J. Automated Measurement of Fracture Callus in Radiographs Using Portable Software. *J. Orthop. Res.* **2016**, *34*, 1224−1233.
(194) Augat, P.; Morgan, E. F.; Lujan, T. J.; MacGillivray, T. J.; Cheung, W. H. Imaging Techniques for the Assessment of Fracture Repair. *Injury* **2014**, *45*, S16−22.
(195) Mehta, M.; Checa, S.; Lienau, J.; Hutmacher, D.; Duda, G. N. In Vivo Tracking of Segmental Bone Defect Healing Reveals That Callus Patterning Is Related to Early Mechanical Stimuli. *Eur. Cell Mater.* **2012**, *24*, 358−371 discussion 371.
(196) Horger, M.; Ditt, H.; Liao, S.; Weisel, K.; Fritz, J.; Thaiss, W. M.; Kaufmann, S.; Nikolaou, K.; Kloth, C. Automated "Bone Subtraction" Image Analysis Software Package for Improved and Faster Ct Monitoring of Longitudinal Spine Involvement in Patients with Multiple Myeloma. *Acad. Radiol* **2017**, *24*, 623−632.
(197) Chen, C. W.; Betz, M. W.; Fisher, J. P.; Paek, A.; Chen, Y. Macroporous Hydrogel Scaffolds and Their Characterization by Optical Coherence Tomography. *Tissue Eng., Part C* **2011**, *17*, 101−112.
(198) Liang, X.; Graf, B. W.; Boppart, S. A. Imaging Engineered Tissues Using Structural and Functional Optical Coherence Tomography. *J. Biophotonics* **2009**, *2*, 643−655.
(199) Zheng, K.; Rupnick, M. A.; Liu, B.; Brezinski, M. E. Three Dimensional Oct in the Engineering of Tissue Constructs: A Potentially Powerful Tool for Assessing Optimal Scaffold Structure. *Open Tissue Eng. Regener. Med. J.* **2009**, *2*, 8−13.
(200) Tan, W.; Oldenburg, A. L.; Norman, J. J.; Desai, T. A.; Boppart, S. A. Optical Coherence Tomography of Cell Dynamics in Three-Dimensional Tissue Models. *Opt. Express* **2006**, *14*, 7159−7171.
(201) Smith, L. E.; Smallwood, R.; Macneil, S. A Comparison of Imaging Methodologies for 3d Tissue Engineering. *Microsc. Res. Tech.* **2010**, *73*, 1123−1133.
(202) Benninger, R. K. P.; Piston, D. W. Two-Photon Excitation Microscopy for the Study of Living Cells and Tissues. *Curr. Protoc. Cell Biol.* **2013**, *59*, 4.11.1.
(203) Guzzi, E. A.; Bovone, G.; Tibbitt, M. W. Universal Nanocarrier Ink Platform for Biomaterials Additive Manufacturing. *Small* **2019**, *15*, 1905421.
(204) Abbadessa, A.; Blokzijl, M. M.; Mouser, V. H.; Marica, P.; Malda, J.; Hennink, W. E.; Vermonden, T. A Thermo-Responsive and Photo-Polymerizable Chondroitin Sulfate-Based Hydrogel for 3d Printing Applications. *Carbohydr. Polym.* **2016**, *149*, 163−174.
(205) Jiang, Y.; De La Cruz, J. A.; Ding, L.; Wang, B.; Feng, X.; Mao, Z.; Xu, H.; Sui, X. Rheology of Regenerated Cellulose Suspension and Influence of Sodium Alginate. *Int. J. Biol. Macromol.* **2020**, *148*, 811.
(206) Diloksumpan, P.; de Ruijter, M.; Castilho, M.; Gbureck, U.; Vermonden, T.; van Weeren, P. R.; Malda, J.; Levato, R. Combining Multi-Scale 3d Printing Technologies to Engineer Reinforced Hydrogel-Ceramic Interfaces. *Biofabrication* **2020**, *12*, 025014.
(207) Blaeser, A.; Duarte Campos, D. F.; Puster, U.; Richtering, W.; Stevens, M. M.; Fischer, H. Controlling Shear Stress in 3d Bioprinting Is a Key Factor to Balance Printing Resolution and Stem Cell Integrity. *Adv. Healthcare Mater.* **2016**, *5*, 326−333.
(208) Ouyang, L.; Highley, C. B.; Sun, W.; Burdick, J. A. A Generalizable Strategy for the 3d Bioprinting of Hydrogels from Nonviscous Photo-Crosslinkable Inks. *Adv. Mater.* **2017**, *29*, 1604983.
(209) Nyberg, E.; Rindone, A.; Dorafshar, A.; Grayson, W. L. Comparison of 3d-Printed Poly-Varepsilon-Caprolactone Scaffolds Functionalized with Tricalcium Phosphate, Hydroxyapatite, Bio-Oss, or Decellularized Bone Matrix. *Tissue Eng., Part A* **2017**, *23*, 503−514.
(210) Moses, J. C.; Saha, T.; Mandal, B. B. Chondroprotective and Osteogenic Effects of Silk-Based Bioinks in Developing 3d Bioprinted Osteochondral Interface. *Bioprinting* **2020**, *17*, e00067.
(211) Yuk, H.; Zhao, X. 3d Printing: A New 3d Printing Strategy by Harnessing Deformation, Instability, and Fracture of Viscoelastic Inks. *Adv. Mater.* **2018**, *30*, 1870037.
(212) Menon, A.; Póczos, B.; Feinberg, A. W.; Washburn, N. R. Optimization of Silicone 3d Printing with Hierarchical Machine Learning. *3D Printing and Additive Manufacturing* **2019**, *6*, 181−189.
(213) Lee, J.; Oh, S. J.; An, S. H.; Kim, W. D.; Kim, S. H. Machine Learning-Based Design Strategy for 3d Printable Bioink: Elastic

https://dx.doi.org/10.1021/acs.chemrev.0c00084
Chem. Rev. 2020, 120, 11028−11055

Modulus and Yield Stress Determine Printability. *Biofabrication* **2020**, *12*, 035018.
(214) Lee, M.; Bae, K.; Guillon, P.; Chang, J.; Arlov, O.; Zenobi-Wong, M. Exploitation of Cationic Silica Nanoparticles for Bioprinting of Large-Scale Constructs with High Printing Fidelity. *ACS Appl. Mater. Interfaces* **2018**, *10*, 37820−37828.
(215) Appel, E. A.; Tibbitt, M. W.; Webber, M. J.; Mattix, B. A.; Veiseh, O.; Langer, R. Self-Assembled Hydrogels Utilizing Polymer-Nanoparticle Interactions. *Nat. Commun.* **2015**, *6*, 6295.
(216) Jalili, N. A.; Jaiswal, M. K.; Peak, C. W.; Cross, L. M.; Gaharwar, A. K. Injectable Nanoengineered Stimuli-Responsive Hydrogels for on-Demand and Localized Therapeutic Delivery. *Nanoscale* **2017**, *9*, 15379−15389.
(217) Liu, B.; Li, J.; Lei, X.; Cheng, P.; Song, Y.; Gao, Y.; Hu, J.; Wang, C.; Zhang, S.; Li, D.; et al. 3d-Bioprinted Functional and Biomimetic Hydrogel Scaffolds Incorporated with Nanosilicates to Promote Bone Healing in Rat Calvarial Defect Model. *Mater. Sci. Eng., C* **2020**, *112*, 110905.
(218) Hausmann, M. K.; Ruhs, P. A.; Siqueira, G.; Lauger, J.; Libanori, R.; Zimmermann, T.; Studart, A. R. Dynamics of Cellulose Nanocrystal Alignment During 3d Printing. *ACS Nano* **2018**, *12*, 6926−6937.
(219) Xu, W.; Molino, B. Z.; Cheng, F.; Molino, P. J.; Yue, Z.; Su, D.; Wang, X.; Willfor, S.; Xu, C.; Wallace, G. G. On Low-Concentration Inks Formulated by Nanocellulose Assisted with Gelatin Methacrylate (Gelma) for 3d Printing toward Wound Healing Application. *ACS Appl. Mater. Interfaces* **2019**, *11*, 8838−8848.
(220) Zhai, X.; Ruan, C.; Ma, Y.; Cheng, D.; Wu, M.; Liu, W.; Zhao, X.; Pan, H.; Lu, W. W. 3d-Bioprinted Osteoblast-Laden Nanocomposite Hydrogel Constructs with Induced Microenvironments Promote Cell Viability, Differentiation, and Osteogenesis Both in Vitro and in Vivo. *Adv. Sci. (Weinh)* **2018**, *5*, 1700550.
(221) Jin, Y.; Chai, W.; Huang, Y. Printability Study of Hydrogel Solution Extrusion in Nanoclay Yield-Stress Bath During Printing-Then-Gelation Biofabrication. *Mater. Sci. Eng., C* **2017**, *80*, 313−325.
(222) Gao, Q.; Niu, X.; Shao, L.; Zhou, L.; Lin, Z.; Sun, A.; Fu, J.; Chen, Z.; Hu, J.; Liu, Y.; et al. 3d Printing of Complex Gelma-Based Scaffolds with Nanoclay. *Biofabrication* **2019**, *11*, 035006.
(223) Yang, F.; Tadepalli, V.; Wiley, B. J. 3d Printing of a Double Network Hydrogel with a Compression Strength and Elastic Modulus Greater Than Those of Cartilage. *ACS Biomater. Sci. Eng.* **2017**, *3*, 863−869.
(224) Zhuo, F.; Liu, X.; Gao, Q.; Wang, Y.; Hu, K.; Cai, Q. Injectable Hyaluronan-Methylcellulose Composite Hydrogel Cross-linked by Polyethylene Glycol for Central Nervous System Tissue Engineering. *Mater. Sci. Eng., C* **2017**, *81*, 1−7.
(225) Jessop, Z. M.; Al-Sabah, A.; Gao, N.; Kyle, S.; Thomas, B.; Badiei, N.; Hawkins, K.; Whitaker, I. S. Printability of Pulp Derived Crystal, Fibril and Blend Nanocellulose-Alginate Bioinks for Extrusion 3d Bioprinting. *Biofabrication* **2019**, *11*, 045006.
(226) Schutz, K.; Placht, A. M.; Paul, B.; Bruggemeier, S.; Gelinsky, M.; Lode, A. Three-Dimensional Plotting of a Cell-Laden Alginate/Methylcellulose Blend: Towards Biofabrication of Tissue Engineering Constructs with Clinically Relevant Dimensions. *J. Tissue Eng. Regener. Med.* **2017**, *11*, 1574−1587.
(227) Loebel, C.; Rodell, C. B.; Chen, M. H.; Burdick, J. A. Shear-Thinning and Self-Healing Hydrogels as Injectable Therapeutics and for 3d-Printing. *Nat. Protoc.* **2017**, *12*, 1521−1541.
(228) Melchels, F. P. W.; Blokzijl, M. M.; Levato, R.; Peiffer, Q. C.; de Ruijter, M.; Hennink, W. E.; Vermonden, T.; Malda, J. Hydrogel-Based Reinforcement of 3d Bioprinted Constructs. *Biofabrication* **2016**, *8*, 035004.
(229) Wenz, A.; Janke, K.; Hoch, E.; Tovar, G. E. M.; Borchers, K.; Kluger, P. J. Hydroxyapatite-Modified Gelatin Bioinks for Bone Bioprinting. *BioNanoMaterials* **2016**, *17*, 179.
(230) Shao, L.; Gao, Q.; Xie, C.; Fu, J.; Xiang, M.; He, Y. Synchronous 3d Bioprinting of Large-Scale Cell-Laden Constructs with Nutrient Networks. *Adv. Healthcare Mater.* **2020**, *9*, 1901142.
(231) Xu, B.; Rodenhizer, D.; Lakhani, S.; Zhang, X.; Soleas, J. P.; Ailles, L.; McGuigan, A. P. Patterning Cellular Compartments within Tracer Cultures Using Sacrificial Gelatin Printing. *Biofabrication* **2016**, *8*, 035018.
(232) Ouyang, L.; Armstrong, J. P. K.; Chen, Q.; Lin, Y.; Stevens, M. M. Void-Free 3d Bioprinting for in Situ Endothelialization and Microfluidic Perfusion. *Adv. Funct. Mater.* **2020**, *30*, 1908349.
(233) Kolesky, D. B.; Truby, R. L.; Gladman, A. S.; Busbee, T. A.; Homan, K. A.; Lewis, J. A. 3d Bioprinting of Vascularized, Heterogeneous Cell-Laden Tissue Constructs. *Adv. Mater.* **2014**, *26*, 3124−3130.
(234) Levato, R.; Webb, W. R.; Otto, I. A.; Mensinga, A.; Zhang, Y.; van Rijen, M.; van Weeren, R.; Khan, I. M.; Malda, J. The Bio in the Ink: Cartilage Regeneration with Bioprintable Hydrogels and Articular Cartilage-Derived Progenitor Cells. *Acta Biomater.* **2017**, *61*, 41−53.
(235) Contessi Negrini, N.; Bonnetier, M.; Giatsidis, G.; Orgill, D. P.; Fare, S.; Marelli, B. Tissue-Mimicking Gelatin Scaffolds by Alginate Sacrificial Templates for Adipose Tissue Engineering. *Acta Biomater.* **2019**, *87*, 61−75.
(236) Compaan, A. M.; Christensen, K.; Huang, Y. Inkjet Bioprinting of 3d Silk Fibroin Cellular Constructs Using Sacrificial Alginate. *ACS Biomater. Sci. Eng.* **2017**, *3*, 1519−1526.
(237) McCormack, A.; Highley, C. B.; Leslie, N. R.; Melchels, F. P. W. 3d Printing in Suspension Baths: Keeping the Promises of Bioprinting Afloat. *Trends Biotechnol.* **2020**, *38*, 584−593.
(238) Wang, Z.; Florczyk, S. J. Freeze-Fresh: A 3d Printing Technique to Produce Biomaterial Scaffolds with Hierarchical Porosity. *Materials* **2020**, *13*, 354.
(239) Bordoni, M.; Karabulut, E.; Kuzmenko, V.; Fantini, V.; Pansarasa, O.; Cereda, C.; Gatenholm, P. 3d Printed Conductive Nanocellulose Scaffolds for the Differentiation of Human Neuroblastoma Cells. *Cells* **2020**, *9*, 682.
(240) Liu, W.; Zhong, Z.; Hu, N.; Zhou, Y.; Maggio, L.; Miri, A. K.; Fragasso, A.; Jin, X.; Khademhosseini, A.; Zhang, Y. S. Coaxial Extrusion Bioprinting of 3d Microfibrous Constructs with Cell-Favorable Gelatin Methacryloyl Microenvironments. *Biofabrication* **2018**, *10*, 024102.
(241) Wang, X.; Li, X.; Dai, X.; Zhang, X.; Zhang, J.; Xu, T.; Lan, Q. Coaxial Extrusion Bioprinted Shell-Core Hydrogel Microfibers Mimic Glioma Microenvironment and Enhance the Drug Resistance of Cancer Cells. *Colloids Surf., B* **2018**, *171*, 291−299.
(242) Gao, Q.; He, Y.; Fu, J. Z.; Liu, A.; Ma, L. Coaxial Nozzle-Assisted 3d Bioprinting with Built-in Microchannels for Nutrients Delivery. *Biomaterials* **2015**, *61*, 203−215.
(243) Pi, Q.; Maharjan, S.; Yan, X.; Liu, X.; Singh, B.; van Genderen, A. M.; Robledo-Padilla, F.; Parra-Saldivar, R.; Hu, N.; Jia, W.; et al. Digitally Tunable Microfluidic Bioprinting of Multilayered Cannular Tissues. *Adv. Mater.* **2018**, *30*, 1706913.
(244) Galarraga, J. H.; Kwon, M. Y.; Burdick, J. A. 3d Bioprinting Via an in Situ Crosslinking Technique Towards Engineering Cartilage Tissue. *Sci. Rep.* **2019**, *9*, 19987.
(245) *ASTM52900-15, I.*; ASTM International: West Conshohocken, PA, 2015.
(246) Raman, R.; Bhaduri, B.; Mir, M.; Shkumatov, A.; Lee, M. K.; Popescu, G.; Kong, H.; Bashir, R. High-Resolution Projection Microstereolithography for Patterning of Neovasculature. *Adv. Healthcare Mater.* **2016**, *5*, 610−619.
(247) Lim, K. S.; Levato, R.; Costa, P. F.; Castilho, M. D.; Alcala-Orozco, C. R.; van Dorenmalen, K. M. A.; Melchels, F. P. W.; Gawlitta, D.; Hooper, G. J.; Malda, J.; et al. Bio-Resin for High Resolution Lithography-Based Biofabrication of Complex Cell-Laden Constructs. *Biofabrication* **2018**, *10*, 034101.
(248) Melchels, F. P.; Feijen, J.; Grijpma, D. W. A Poly(D,L-Lactide) Resin for the Preparation of Tissue Engineering Scaffolds by Stereolithography. *Biomaterials* **2009**, *30*, 3801−3809.
(249) Qiu, B.; Bessler, N.; Figler, K.; Buchholz, M. B.; Rios, A. C.; Malda, J.; Levato, R.; Caiazzo, M. Bioprinting Neural Systems to

https://dx.doi.org/10.1021/acs.chemrev.0c00084
Chem. Rev. 2020, 120, 11028−11055

Model Central Nervous System Diseases. *Adv. Funct. Mater.* **2020**, 1910250.
(250) Kunwar, P.; Xiong, Z.; Zhu, Y.; Li, H.; Filip, A.; Soman, P. Hybrid Laser Printing of 3d, Multiscale, Multimaterial Hydrogel Structures. *Adv. Opt. Mater.* **2019**, *7*, 1900656.
(251) Dobos, A.; Van Hoorick, J.; Steiger, W.; Gruber, P.; Markovic, M.; Andriotis, O. G.; Rohatschek, A.; Dubruel, P.; Thurner, P. J.; Van Vlierberghe, S.; Baudis, S.; Ovsianikov, A. Thiol-Gelatin-Norbornene Bioink for Laser-Based High-Definition Bioprinting. *Adv. Healthcare Mater.* **2020**, *9*, 1900752.
(252) Mondschein, R. J.; Kanitkar, A.; Williams, C. B.; Verbridge, S. S.; Long, T. E. Polymer Structure-Property Requirements for Stereolithographic 3d Printing of Soft Tissue Engineering Scaffolds. *Biomaterials* **2017**, *140*, 170−188.
(253) Bertlein, S.; Brown, G.; Lim, K. S.; Jungst, T.; Boeck, T.; Blunk, T.; Tessmar, J.; Hooper, G. J.; Woodfield, T. B. F.; Groll, J. Thiol-Ene Clickable Gelatin: A Platform Bioink for Multiple 3d Biofabrication Technologies. *Adv. Mater.* **2017**, *29*, 1703404.
(254) Raman, R.; Clay, N. E.; Sen, S.; Melhem, M.; Qin, E.; Kong, H.; Bashir, R. 3d Printing Enables Separation of Orthogonal Functions within a Hydrogel Particle. *Biomed. Microdevices* **2016**, *18*, 49.
(255) Wang, Z.; Abdulla, R.; Parker, B.; Samanipour, R.; Ghosh, S.; Kim, K. A Simple and High-Resolution Stereolithography-Based 3d Bioprinting System Using Visible Light Crosslinkable Bioinks. *Biofabrication* **2015**, *7*, 045009.
(256) Bajaj, P.; Marchwiany, D.; Duarte, C.; Bashir, R. Patterned Three-Dimensional Encapsulation of Embryonic Stem Cells Using Dielectrophoresis and Stereolithography. *Adv. Healthcare Mater.* **2013**, *2*, 450−458.
(257) Palaganas, N. B.; Mangadlao, J. D.; de Leon, A. C. C.; Palaganas, J. O.; Pangilinan, K. D.; Lee, Y. J.; Advincula, R. C. 3d Printing of Photocurable Cellulose Nanocrystal Composite for Fabrication of Complex Architectures Via Stereolithography. *ACS Appl. Mater. Interfaces* **2017**, *9*, 34314−34324.
(258) Sharifi, S.; Blanquer, S. B.; van Kooten, T. G.; Grijpma, D. W. Biodegradable Nanocomposite Hydrogel Structures with Enhanced Mechanical Properties Prepared by Photo-Crosslinking Solutions of Poly(Trimethylene Carbonate)-Poly(Ethylene Glycol)-Poly-(Trimethylene Carbonate) Macromonomers and Nanoclay Particles. *Acta Biomater.* **2012**, *8*, 4233−4243.
(259) Zhou, X.; Zhu, W.; Nowicki, M.; Miao, S.; Cui, H.; Holmes, B.; Glazer, R. I.; Zhang, L. G. 3d Bioprinting a Cell-Laden Bone Matrix for Breast Cancer Metastasis Study. *ACS Appl. Mater. Interfaces* **2016**, *8*, 30017−30026.
(260) Tromayer, M.; Gruber, P.; Markovic, M.; Rosspeintner, A.; Vauthey, E.; Redl, H.; Ovsianikov, A.; Liska, R. A Biocompatible Macromolecular Two-Photon Initiator Based on Hyaluronan. *Polym. Chem.* **2017**, *8*, 451−460.
(261) Gauvin, R.; Chen, Y. C.; Lee, J. W.; Soman, P.; Zorlutuna, P.; Nichol, J. W.; Bae, H.; Chen, S.; Khademhosseini, A. Microfabrication of Complex Porous Tissue Engineering Scaffolds Using 3d Projection Stereolithography. *Biomaterials* **2012**, *33*, 3824−3834.
(262) Wu, Y.; Chen, Y. X.; Yan, J.; Quinn, D.; Dong, P.; Sawyer, S. W.; Soman, P. Fabrication of Conductive Gelatin Methacrylate-Polyaniline Hydrogels. *Acta Biomater.* **2016**, *33*, 122−130.
(263) Kim, S. H.; Yeon, Y. K.; Lee, J. M.; Chao, J. R.; Lee, Y. J.; Seo, Y. B.; Sultan, M. T.; Lee, O. J.; Lee, J. S.; Yoon, S. I.; et al. Precisely Printable and Biocompatible Silk Fibroin Bioink for Digital Light Processing 3d Printing. *Nat. Commun.* **2018**, *9*, 1620.
(264) Della Giustina, G.; Gandin, A.; Brigo, L.; Panciera, T.; Giulitti, S.; Sgarbossa, P.; D'Alessandro, D.; Trombi, L.; Danti, S.; Brusatin, G. Polysaccharide Hydrogels for Multiscale 3d Printing of Pullulan Scaffolds. *Mater. Des.* **2019**, *165*, 107566.
(265) Van Hoorick, J.; Gruber, P.; Markovic, M.; Rollot, M.; Graulus, G. J.; Vagenende, M.; Tromayer, M.; Van Erps, J.; Thienpont, H.; Martins, J. C.; et al. Highly Reactive Thiol-Norbornene Photo-Click Hydrogels: Toward Improved Processability. *Macromol. Rapid Commun.* **2018**, *39*, 1800181.
(266) Valentin, T. M.; Leggett, S. E.; Chen, P. Y.; Sodhi, J. K.; Stephens, L. H.; McClintock, H. D.; Sim, J. Y.; Wong, I. Y. Stereolithographic Printing of Ionically-Crosslinked Alginate Hydrogels for Degradable Biomaterials and Microfluidics. *Lab Chip* **2017**, *17*, 3474−3488.
(267) Vaezi, M.; Seitz, H.; Yang, S. A Review on 3d Micro-Additive Manufacturing Technologies. *International Journal of Advanced Manufacturing Technology* **2013**, *67*, 1721−1754.
(268) Seck, T. M.; Melchels, F. P. W.; Feijen, J.; Grijpma, D. W. Designed Biodegradable Hydrogel Structures Prepared by Stereolithography Using Poly(Ethylene Glycol)/Poly(D,L-Lactide)-Based Resins. *J. Controlled Release* **2010**, *148*, 34−41.
(269) Dwyer, S. F.; Gelman, I. H. Cross-Phosphorylation and Interaction between Src/Fak and Mapkap5/Prak in Early Focal Adhesions Controls Cell Motility. *J. Cancer Biol. Res.* **2014**, *2*, 1045.
(270) Shin, S.; Kwak, H.; Hyun, J. Melanin Nanoparticle-Incorporated Silk Fibroin Hydrogels for the Enhancement of Printing Resolution in 3d-Projection Stereolithography of Poly(Ethylene Glycol)-Tetraacrylate Bio-Ink. *ACS Appl. Mater. Interfaces* **2018**, *10*, 23573−23582.
(271) Li, Z. Q.; Torgersen, J.; Ajami, A.; Muhleder, S.; Qin, X. H.; Husinsky, W.; Holnthoner, W.; Ovsianikov, A.; Stampfl, J.; Liska, R. Initiation Efficiency and Cytotoxicity of Novel Water-Soluble Two-Photon Photoinitiators for Direct 3d Microfabrication of Hydrogels. *RSC Adv.* **2013**, *3*, 15939−15946.
(272) Chu, S.; Maples, M. M.; Bryant, S. J. Cell Encapsulation Spatially Alters Crosslink Density of Poly(Ethylene Glycol) Hydrogels Formed from Free-Radical Polymerizations. *Acta Biomater.* **2020**, *109*, 37−50.
(273) Egbu, R.; Brocchini, S.; Khaw, P. T.; Awwad, S. Antibody Loaded Collapsible Hyaluronic Acid Hydrogels for Intraocular Delivery. *Eur. J. Pharm. Biopharm.* **2018**, *124*, 95−103.
(274) de Almeida Monteiro Melo Ferraz, M.; Henning, H. H. W.; Ferreira da Costa, P.; Malda, J.; Le Gac, S.; Bray, F.; van Duursen, M. B. M.; Brouwers, J. F.; van de Lest, C. H. A.; Bertijn, I.; et al. Potential Health and Environmental Risks of Three-Dimensional Engineered Polymers. *Environ. Sci. Technol. Lett.* **2018**, *5*, 80−85.
(275) Cvetkovic, C.; Raman, R.; Chan, V.; Williams, B. J.; Tolish, M.; Bajaj, P.; Sakar, M. S.; Asada, H. H.; Saif, M. T.; Bashir, R. Three-Dimensionally Printed Biological Machines Powered by Skeletal Muscle. *Proc. Natl. Acad. Sci. U. S. A.* **2014**, *111*, 10125−10130.
(276) Chan, V.; Jeong, J. H.; Bajaj, P.; Collens, M.; Saif, T.; Kong, H.; Bashir, R. Multi-Material Bio-Fabrication of Hydrogel Cantilevers and Actuators with Stereolithography. *Lab Chip* **2012**, *12*, 88−98.
(277) Miller, A. T.; Safranski, D. L.; Wood, C.; Guldberg, R. E.; Gall, K. Deformation and Fatigue of Tough 3d Printed Elastomer Scaffolds Processed by Fused Deposition Modeling and Continuous Liquid Interface Production. *J. Mech Behav Biomed Mater.* **2017**, *75*, 1−13.
(278) Tumbleston, J. R.; Shirvanyants, D.; Ermoshkin, N.; Janusziewicz, R.; Johnson, A. R.; Kelly, D.; Chen, K.; Pinschmidt, R.; Rolland, J. P.; Ermoshkin, A.; et al. Additive Manufacturing. Continuous Liquid Interface Production of 3d Objects. *Science* **2015**, *347*, 1349−1352.
(279) Yin, H.; Ding, Y.; Zhai, Y.; Tan, W.; Yin, X. Orthogonal Programming of Heterogeneous Micro-Mechano-Environments and Geometries in Three-Dimensional Bio-Stereolithography. *Nat. Commun.* **2018**, *9*, 4096.
(280) Nam, S. Y.; Park, S. H. Ecm Based Bioink for Tissue Mimetic 3d Bioprinting. *Adv. Exp. Med. Biol.* **2018**, *1064*, 335−353.
(281) Jessop, Z. M.; Al-Sabah, A.; Gardiner, M. D.; Combellack, E.; Hawkins, K.; Whitaker, I. S. 3d Bioprinting for Reconstructive Surgery: Principles, Applications and Challenges. *J. Plast Reconstr Aesthet Surg* **2017**, *70*, 1155−1170.
(282) Chimene, D.; Lennox, K. K.; Kaunas, R. R.; Gaharwar, A. K. Advanced Bioinks for 3d Printing: A Materials Science Perspective. *Ann. Biomed. Eng.* **2016**, *44*, 2090−2102.
(283) Gladman, A. S.; Matsumoto, E. A.; Nuzzo, R. G.; Mahadevan, L.; Lewis, J. A. Biomimetic 4d Printing. *Nat. Mater.* **2016**, *15*, 413−418.

https://dx.doi.org/10.1021/acs.chemrev.0c00084
Chem. Rev. 2020, 120, 11028−11055

(284) Kirillova, A.; Maxson, R.; Stoychev, G.; Gomillion, C. T.; Ionov, L. 4d Biofabrication Using Shape-Morphing Hydrogels. *Adv. Mater.* **2017**, *29*, 1703443.
(285) Yang, Q.; Gao, B.; Xu, F. Recent Advances in 4d Bioprinting. *Biotechnol. J.* **2020**, *15*, 1900086.
(286) Wan, Z.; Zhang, P.; Liu, Y.; Lv, L.; Zhou, Y. Four-Dimensional Bioprinting: Current Developments and Applications in Bone Tissue Engineering. *Acta Biomater.* **2020**, *101*, 26−42.
(287) Tamay, D. G.; Usal, T. D.; Alagoz, A. S.; Yucel, D.; Hasirci, N.; Hasirci, V. 3d and 4d Printing of Polymers for Tissue Engineering Applications. *Front. Bioeng. Biotechnol.* **2019**, *7*, 164.
(288) Lewis, P. L.; Green, R. M.; Shah, R. N. 3d-Printed Gelatin Scaffolds of Differing Pore Geometry Modulate Hepatocyte Function and Gene Expression. *Acta Biomater.* **2018**, *69*, 63−70.
(289) Martin, I.; Malda, J.; Rivron, N. C. Organs by Design: Can Bioprinting Meet Self-Organization? *Curr. Opin. Organ Transplant.* **2019**, *24*, 562−567.
(290) Colosi, C.; Shin, S. R.; Manoharan, V.; Massa, S.; Costantini, M.; Barbetta, A.; Dokmeci, M. R.; Dentini, M.; Khademhosseini, A. Microfluidic Bioprinting of Heterogeneous 3d Tissue Constructs Using Low-Viscosity Bioink. *Adv. Mater.* **2016**, *28*, 677−684.

https://dx.doi.org/10.1021/acs.chemrev.0c00084
Chem. Rev. 2020, 120, 11028−11055